been proposed for early-phase diffuse cutaneous SSc [9], patients are at risk of developing sclerodermal renal crisis [10]. The effectiveness of penicillamine in SSc treatment remains controversial [11]. On the other hand, the European League Against Rheumatism recommends methotrexate for treatment of skin sclerosis in patients with early diffuse SSc [12], but an opposing view was also presented [13]. Other immunosuppressive agents such as cyclophosphamide, cyclosporine A, tacrolimus, and mycophenolate mofetil have been evaluated for treatment of SSc. Though the beneficial effects of one-year oral administration of cyclophosphamide on skin thickening have been reported [14], the long-term safety of this medicine has not been verified. There are no data which present late-occurring toxicities of cyclophosphamide in patients with SSc, but there are several reports which present oncogenicity after withdrawal of this medicine in patients with systemic lupus erythematosus and rheumatoid arthritis [15]. The usefulness of cyclosporine is also controversial because of the associated risk of sclerodermal renal crisis [16, 17]. The effectiveness of mycophenolate mofetil as an immunosuppressive agent in SSc treatment also remains inconclusive [18, 19], though a recent study presented beneficial effects in patients with recent-onset SSc [20]. Finally, several biologic agents are currently being evaluated for treatment of skin involvement in SSc, of which only rituximab has shown efficacy [21, 22]. Therefore, effective treatment for this disease is an ongoing challenge.

The effect of TCZ on skin sclerosis, pneumonitis, or the other symptoms in patients with SSc remains unclear, and further studies are required to verify this. The efficacy of TCZ for patients with SSc is currently being evaluated in an open-label trial in Japan (UMIN0000055550) and a double-blind trial in Europe and North America (NCT01532869); the results of these trials should provide further information on unresolved issues.

In this report, we described time-course changes of ROM observed in a patient with SSc during treatment with TCZ. The relation between TCZ treatment and ROM changes observed in the patient is currently unclear.

Downloaded by [Osaka University] at 16:57 07 February 2016

## Acknowledgments

Our heartfelt appreciation goes to Dr. Kuwahara, Dr. Watanabe, and Dr. Kawai, whose outstanding medical work was of inestimable value for our study. We are indebted to Dr. Iwatani, Dr. Sakata, Dr. Okano, and Dr. Takahashi, whose extensive knowledge in nephrology, cardiology, and gastroenterology made an enormous contribution to our work. This work was supported by the Program for Promotion of Fundamental Studies in Health Sciences of the National Institute of Biomedical Innovation, Japan.

## Conflict of interest

T. Kishimoto holds a patent for TCZ, and receives royalties for ACTEMRA®. A. Ogata received a consulting fee from Chugai Pharmaceutical Co. Ltd. for providing medical advice. Other authors have no conflict of interest to declare.

## References

1. Gurram M, Pahwa S, Frieri M. Augmented interleukin-6 secretion in collagen-stimulated peripheral blood mononuclear cells from patients with systemic sclerosis. Ann Allergy. 1994;73:493–6.
2. Feghali CA, Bost KL, Boulware DW, Levy LS. Mechanisms of pathogenesis in scleroderma. I. Overproduction of interleukin 6 by fibroblasts cultured from affected skin sites of patients with scleroderma. J Rheumatol. 1992;19:1207–11.
3. Hasegawa M, Sato S, Fujimoto M, Ihn H, Kikuchi K, Takehara K. Serum levels of interleukin 6 (IL-6), oncostatin M, soluble IL-6 receptor, and soluble gp130 in patients with systemic sclerosis. J Rheumatol. 1998;25:308–13.
4. Sato S, Hasegawa M, Takehara K. Serum levels of interleukin-6 and interleukin-10 correlate with total skin thickness score in patients with systemic sclerosis. J Dermatol Sci. 2001;27:140–6.
5. Khan K, Xu S, Nihtyanova S, Derrett-Smith E, Abraham D, Denton CP, Ong VH. Clinical and pathological significance of interleukin 6 overexpression in systemic sclerosis. Ann Rheum Dis. 2012 [Epub ahead of print].
6. Kawaguchi Y, Hara M, Wright TM. Endogenous IL-1alpha from systemic sclerosis fibroblasts induces IL-6 and PDGF-A. J Clin Invest. 1999;103:1253–60.
7. Shima Y, Kuwahara Y, Murota H, Kitaba S, Kawai M, Hirano T, Arimitsu J, Narazaki M, Hagihara K, Ogata A, Katayama I, Kawase I, Kishimoto T, Tanaka T. The skin of patients with systemic sclerosis softened during the treatment with anti-IL-6 receptor antibody tocilizumab. Rheumatology (Oxford). 2010;49:2408–12.
8. Kuhn A, Haust M, Ruland V, Weber R, Verde P, Felder G, Ohmann C, Gensch K, Ruzicka T. Effect of bosentan on skin fibrosis in patients with systemic sclerosis: a prospective, open-label, non-comparative trial. Rheumatology (Oxford). 2010;49:1336–45.
9. Takehara K. Treatment of early diffuse cutaneous systemic sclerosis patients in Japan by low-dose corticosteroids for skin involvement. Clin Exp Rheumatol. 2004;22:S87–9.
10. Steen VD, Medsger TA Jr. Case-control study of corticosteroids and other drugs that either precipitate or protect from the development of scleroderma renal crisis. Arthr Rheum. 1998;41:1613–9.
11. Clements PJ, Furst DE, Wong WK, Mayes M, White B, Wigley F, Weisman MH, Barr W et al. High-dose versus low-dose D-penicillamine in early diffuse systemic sclerosis: analysis of a two-year, double-blind, randomized, controlled clinical trial. Arthr Rheum. 1999;42:1194–203.
12. Kowal-Bielecka O, Landewé R, Avouac J, Chwiesko S, Miniati I, Czirjak L, Clements P, Denton C et al. EULAR recommendations for the treatment of systemic sclerosis a report from the EULAR Scleroderma Trials and Research group (EUSTAR). Ann Rheum Dis. 2009;68:620–8.
13. Pope JE, Bellamy N, Seibold JR, Baron M, Ellman M, Carette S, Smith CD, Chalmers IM, Hong P, O'Hanlon D, Kaminska E, Markland J, Sibley J, Catoggio L, Furst DE. A randomized, controlled trial of methotrexate versus placebo in early diffuse scleroderma. Arthr Rheum. 2001;44:1351–8.
14. Tashkin DP, Elashoff R, Clements PJ, Goldin J, Roth MD, Furst DE, Arriola E, Silver Ret al. Cyclophosphamide versus placebo in scleroderma lung disease. N Engl J Med. 2006;354:2655–66.
15. Plotz PH, Klippel JH, Decker JL, Grauman D, Wolff B, Brown BC, Rutt G. Bladder complications in patients receiving cyclophosphamide for systemic lupus erythematosus or rheumatoid arthritis. Ann Intern Med. 1979;91:221–3.
16. Filaci G, Cutolo M, Scudeletti M, Castagneto C, Derchi L, Gianrossi R, Ropolo F, Zentilin P, Sulli A, Murdaca G, Ghio M, Indiveri F, Puppo F. Cyclosporin A and iloprost treatment of systemic sclerosis: clinical results and interleukin-6 serum changes after 12 months of therapy. Rheumatology (Oxford). 1999;38:992–6.
17. Denton CP, Sweny P, Abdulla A, Black CM. Acute renal failure occurring in scleroderma treated with cyclosporin A: a report of three cases. Br J Rheumatol. 1994;33:90–2.
18. Stratton RJ, Wilson H, Black CM. Pilot study of anti-thymocyte globulin plus mycophenolate mofetil in recent-onset diffuse scleroderma. Rheumatology (Oxford). 2001;40:84–8.
19. Nihtyanova SI, Brough GM, Black CM, Denton CP. Mycophenolate mofetil in diffuse cutaneous systemic sclerosis–a retrospective analysis. Rheumatology (Oxford). 2007;46:442–5.
20. Mendoza FA, Nagle SJ, Lee JB, Jimenez SA. A prospective observational study of mycophenolate mofetil treatment in progressive diffuse cutaneous systemic sclerosis of recent onset. J Rheumatol. 2012;39:1241–7.
21. Denton CP, Engelhart M, Tvede N, Wilson H, Khan K, Shiwen X, Carreira PE, Diaz Gonzalez F, Black CM, Hoogen FH. An open-label pilot study of infliximab therapy in diffuse cutaneous systemic sclerosis. Ann Rheum Dis. 2009;68:1433–9.
22. McGonagle D, Tan AL, Madden J, Rawstron AC, Rehman A, Emery P, Thomas S. Successful treatment of resistant scleroderma-associated interstitial lung disease with rituximab. Rheumatology (Oxford). 2008;47:552–3.

# Interleukin-6/interleukin-21 signaling axis is critical in the pathogenesis of pulmonary arterial hypertension

Takahiro Hashimoto-Kataoka[a], Naoki Hosen[b], Takashi Sonobe[c], Yoh Arita[a], Taku Yasui[a], Takeshi Masaki[a], Masato Minami[d], Tadakatsu Inagaki[c], Shigeru Miyagawa[e], Yoshiki Sawa[e], Masaaki Murakami[f], Atsushi Kumanogoh[g], Keiko Yamauchi-Takihara[a], Meinoshin Okumura[d], Tadamitsu Kishimoto[h], Issei Komuro[i,j], Mikiyasu Shirai[c], Yasushi Sakata[a], and Yoshikazu Nakaoka[a,k,1]

Departments of [a]Cardiovascular Medicine, [b]Cancer Stem Cell Biology Functional Diagnostic Science, [d]General Thoracic Surgery, [e]Cardiovascular Surgery, and [g]Respiratory Medicine, Allergy and Rheumatic Disease, Osaka University Graduate School of Medicine, Suita, Osaka, 565-0871, Japan; [c]Department of Cardiac Physiology, National Cerebral and Cardiovascular Center Research Institute, Suita, Osaka, 565-8565, Japan; [f]Department of Molecular Neuroimmunology, Institute for Genetic Medicine, Hokkaido University, Sapporo, Hokkaido, 060-0815, Japan; [h]Laboratory of Immune Regulation, Immunology Frontier Research Center, Osaka University, Suita, Osaka, 565-0871, Japan; [i]Department of Cardiovascular Medicine, The University of Tokyo Graduate School of Medicine, Tokyo, 113-8656, Japan; and [j]Core Research for Evolutional Science and Technology and [k]Precursory Research for Embryonic Science and Technology, Japan Science Technology Agency, Kawaguchi, Saitama, 332-0012, Japan

Edited by Kari Alitalo, University of Helsinki, Helsinki, Finland, and approved April 16, 2015 (received for review December 26, 2014)

**IL-6 is a multifunctional proinflammatory cytokine that is elevated in the serum of patients with pulmonary arterial hypertension (PAH) and can predict the survival of patients with idiopathic PAH (IPAH). Previous animal experiments and clinical human studies indicate that IL-6 is important in PAH; however, the molecular mechanisms of IL-6–mediated pathogenesis of PAH have been elusive. Here we identified IL-21 as a downstream target of IL-6 signaling in PAH. First, we found that IL-6 blockade by the monoclonal anti-IL-6 receptor antibody, MR16-1, ameliorated hypoxia-induced pulmonary hypertension (HPH) and prevented the hypoxia-induced accumulation of Th17 cells and M2 macrophages in the lungs. Consistently, the expression levels of IL-17 and IL-21 genes, one of the signature genes for Th17 cells, were significantly up-regulated after hypoxia exposure in the lungs of mice treated with control antibody but not in the lungs of mice treated with MR16-1. Although IL-17 blockade with an anti–IL-17A neutralizing antibody had no effect on HPH, IL-21 receptor-deficient mice were resistant to HPH and exhibited no significant accumulation of M2 macrophages in the lungs. In accordance with these findings, IL-21 promoted the polarization of primary alveolar macrophages toward the M2 phenotype. Of note, significantly enhanced expressions of IL-21 and M2 macrophage markers were detected in the lungs of IPAH patients who underwent lung transplantation. Collectively, these findings suggest that IL-21 promotes PAH in association with M2 macrophage polarization, downstream of IL-6-signaling. The IL-6/IL-21–signaling axis may be a potential target for treating PAH.**

pulmonary arterial hypertension | interleukin-21 | interleukin-6 | Th17 cells | M2 macrophage

Pulmonary arterial hypertension (PAH) is a debilitating disease characterized by arteriopathy in the small to medium-sized distal pulmonary arteries that is associated with arterial muscularization, concentric intimal thickening, and the formation of plexiform lesions (1, 2). Inflammation and autoimmunity currently are recognized as critical contributors to the pathogenesis of PAH (3, 4). Inflammatory cells such as T cells, B cells, and macrophages infiltrate the plexiform lesions in patients with advanced PAH. Thus, proinflammatory cytokines produced by these cells may be responsible for the hyperproliferation of pulmonary artery endothelial cells (PAECs) and pulmonary artery smooth muscle cells (PASMCs) (5, 6).

IL-6 is a multifunctional proinflammatory cytokine linked to numerous autoimmune diseases (7, 8). Patients with idiopathic PAH (IPAH) exhibit increased IL-6 serum levels, which correlate with their prognoses (3, 9, 10). Consistent with these findings, lung-specific IL-6 transgenic mice display spontaneous pulmonary hypertension in normoxia and develop greatly exaggerated hypoxia-induced pulmonary hypertension (HPH) (11), whereas IL-6–deficient mice show resistance to HPH (12). These findings suggest that IL-6 has a significant role in the pathogenesis of pulmonary hypertension; however, the downstream target(s) of IL-6 in HPH have been elusive.

T-helper cells are comprised of three subsets, Th1, Th2, and Th17 cells, which are defined by the cytokines they produce (13, 14). Th17 cells, a subset of IL-17–producing effector T cells, play important roles in the pathogenesis of autoimmune diseases such as rheumatoid arthritis (13, 14). IL-6 together with TGF-β promotes the differentiation of Th17 cells (14, 15). However, the involvement of Th17 cells in the pathogenesis of HPH has not been determined.

Macrophages undergo differential polarization that generates three distinct macrophage populations: the classically activated (M1), alternatively activated (M2), and anti-inflammatory (regulatory) macrophages (16–18). Upon their activation by IFN-γ and TNF-α, M1 macrophages exert microbicidal and tumoricidal effects by producing inducible nitric oxide synthase and IL-12p40

## Significance

Pulmonary arterial hypertension (PAH) is a serious disease characterized by vascular remodeling in pulmonary arteries. Although an elevated IL-6 serum level correlates with poor prognosis of PAH patients, it is unclear how IL-6 promotes PAH. Here we identified IL-21 as a downstream target of IL-6 signaling in PAH. In mice with hypoxia-induced pulmonary hypertension (HPH), Th17 cells and M2 macrophages accumulate in the lungs after hypoxia exposure. IL-21 primarily derived from Th17 cells promotes M2 macrophage polarization. Consistently, IL-21 receptor-deficient mice show resistance to HPH with no accumulation of M2 macrophages in the lungs. IL-21 and M2 macrophage markers were upregulated in the lungs of patients with end-stage idiopathic PAH. These findings suggest promising therapeutic strategies for PAH targeting IL-6/IL-21–signaling axis.

Author contributions: T.H.-K., T.K., I.K., M.S., and Y.N. designed research; T.H.-K., N.H., T.S., Y.A., T.Y., T.M., M. Minami, T.I., S.M., K.Y.-T., M.S., and Y.N. performed research; M. Minami, Y. Sawa, M. Murakami, M.O., and T.K. contributed new reagents/analytic tools; T.H.-K., N.H., T.S., M. Murakami, A.K., K.Y.-T., M.S., Y. Sakata, and Y.N. analyzed data; and T.H.-K. and Y.N. wrote the paper.

Conflict of interest statement: T.K. holds a patent for a monoclonal humanized anti-IL6R antibody (tocilizumab). Y.N. is a consultant of the sponsor-initiated clinical trial (Chugai Pharmaceutical Co.) using tocilizumab for Takayasu arteritis.

This article is a PNAS Direct Submission.

Freely available online through the PNAS open access option.

[1]To whom correspondence should be addressed. Email: ynakaoka@cardiology.med.osaka-u.ac.jp.

This article contains supporting information online at www.pnas.org/lookup/suppl/doi:10.1073/pnas.1424774112/-/DCSupplemental.

(17, 18). In contrast, M2 macrophages are activated by IL-4 and IL-13 and characteristically express arginase-1 (Arg1), found in inflammatory zone-1 (Fizz1), chitinase 3-like-3 (Ym1), and mannose receptor, C type lectin-1 (MRC-1) (16–18). Intriguingly, M2 macrophages recently were reported to play a critical role in HPH (19); however, the molecular mechanisms underlying macrophage polarization in HPH are unknown.

Here, we examined the roles of IL-6 and its downstream signaling targets in the pathogenesis of HPH in mice. We found that the IL-6/IL-21–signaling axis played critical roles in the development of HPH in association with M2 macrophage polarization. Consistent with these findings in mice, large numbers of IL-21$^+$ cells and M2 macrophages were detected in the lungs of patients with IPAH. Taken together, these findings indicate a conserved role for the IL-6/IL-21–signaling axis in mouse HPH and human PAH (HPAH) and suggest promising targets for treating PAH.

## Results

**Hypoxia-Induced IL-6 Expression in Mouse Pulmonary Vessels.** We first examined the *Il-6* mRNA levels in the lungs of C57BL/6 mice after hypoxia exposure using quantitative RT-PCR (qRT-PCR). The *Il-6* mRNA levels peaked on day 2 and returned to basal levels by day 7 after hypoxia exposure (Fig. 1*A*). Consistent with this finding, immunohistochemical analysis demonstrated strong IL-6 induction in the intima and medial layers of the arterioles and small arteries of the lung on day 2 after hypoxia exposure (Fig. 1*B*).

**IL-6 Blockade by MR16-1 Prevents HPH.** IL-6 signaling is transduced primarily by STAT3. Thus, we examined the tyrosine-phosphorylation of STAT3 in the lungs of mice. Although tyrosine-phosphorylation of STAT3 was strongly induced by hypoxia exposure in the lungs of mice treated with control antibody, it was attenuated in those treated with the anti–IL-6 receptor (IL-6R) antibody MR16-1 (Fig. 1*C*). Next, we investigated the effect of IL-6 blockade on HPH development by measuring the right ventricular systolic pressure (RVSP), Fulton's index [right/(left + septum) ventricular weight], and the medial wall thickness index, which is estimated by elastic Van Gieson staining of the pulmonary arterioles (Fig. 1*D*). In control antibody-treated mice, hypoxia exposure for 4 wk induced significant increases in the RVSP, Fulton's index, and medial wall thickness index, compared with the values observed under normoxic conditions (Fig. 1 *E–G*). In contrast, the hypoxia-induced elevation of these parameters was significantly inhibited by treatment with MR16-1 (Fig. 1 *E–G*). Similarly, thickened medial vascular walls were detected in the lung sections of control antibody-treated mice but not in those of mice treated with MR16-1 (Fig. 1*H*). Under normoxia, there was no significant difference in the physiological parameters of mice treated with control antibody and those treated with MR16-1 (Table S1). These data suggest that IL-6 blockade by MR16-1 effectively prevents HPH.

**IL-6 Blockade Abrogates Hypoxia-Induced Accumulation of Th17 Cells in the Lungs.** IL-6–dependent accumulation of Th17 cells promotes the development of inflammatory diseases, such as rheumatoid arthritis (20). Thus, we examined the involvement of Th17 cells in HPH by measuring the mRNA levels of *Il-17A*, a Th17 signature gene. Hypoxia-induced *Il-17A* in the lungs peaked on day 2 and declined on day 7 but remained slightly higher than the basal level on and after day 7 (Fig. 2*A*). We next examined the mRNA levels of *IL-17A* and other Th17 signature gene, such as *Rorc* (*retinoic acid receptor–related orphan receptor-c*, also known as "*Ror-γt*"), and IL-17–downstream chemokines, such as *Cxcl1* and *Cxcl5*, in the lungs of mice exposed to hypoxia for 2 d. The mRNA levels of all these genes were significantly up-regulated in the lungs of control antibody-treated mice but not in those of mice treated with MR16-1 (Fig. 2 *B–E*). The IL-17A protein levels also were increased after hypoxia in the lungs of control antibody-treated mice but not in those of mice treated with MR16-1 (Fig. 2 *F* and *G*). In addition, exposure to hypoxia for 3 d led to significantly increased Th17 numbers in the lungs of control antibody-treated mice but not in those of mice treated with MR16-1 (Fig. 2 *H* and *I*). In contrast, there was no substantial difference in Th1 and Th2 numbers in the lungs of mice

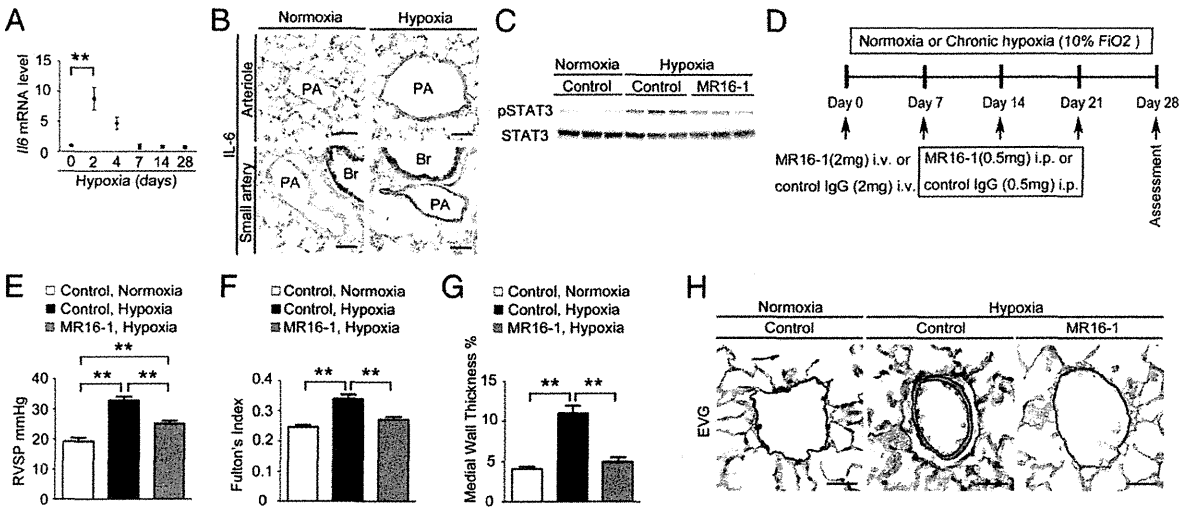


**Fig. 1.** Blockade of IL-6 signaling prevents HPH. (*A*) qRT-PCR analysis of *Il-6* mRNA expression in the lungs of C57BL/6 WT mice after hypoxia exposure. Each data point represents the analysis of 5–10 mice. (*B*) Representative IL-6 immunostaining of lung sections from C57BL6 mice after exposure to hypoxia or normoxia for 2 d ($n = 5$). (*C*) Western blot analysis of STAT3 phosphorylation (Tyr705) and total STAT3 in lung homogenates from mice treated with control antibody or MR16-1 after exposure to normoxia or hypoxia for 2 d ($n = 3$). (*D*) Experimental protocol for examining the effect of antibody treatment on HPH. MR16-1 or control antibody was administered to C57BL/6 mice under normoxic or hypoxic conditions. (*E–G*) Assessment of antibody-treated mice. (*E*) RVSP ($n = 8–12$). (*F*) Fulton's index ($n = 8–12$). (*G*) Medial wall thickness index (percent wall thickness) ($n = 5–6$). Distal acinar arterioles (50–100 μm in diameter) were examined. (*H*) Representative images of the vascular remodeling of distal acinar arterioles in lung sections subjected to elastic Van Gieson (EVG) staining. (Scale bars: 25 μm.) Br, bronchus; PA, pulmonary artery. Values shown are the mean ± SEM; $*P < 0.05$, $**P < 0.01$ calculated using ANOVA.

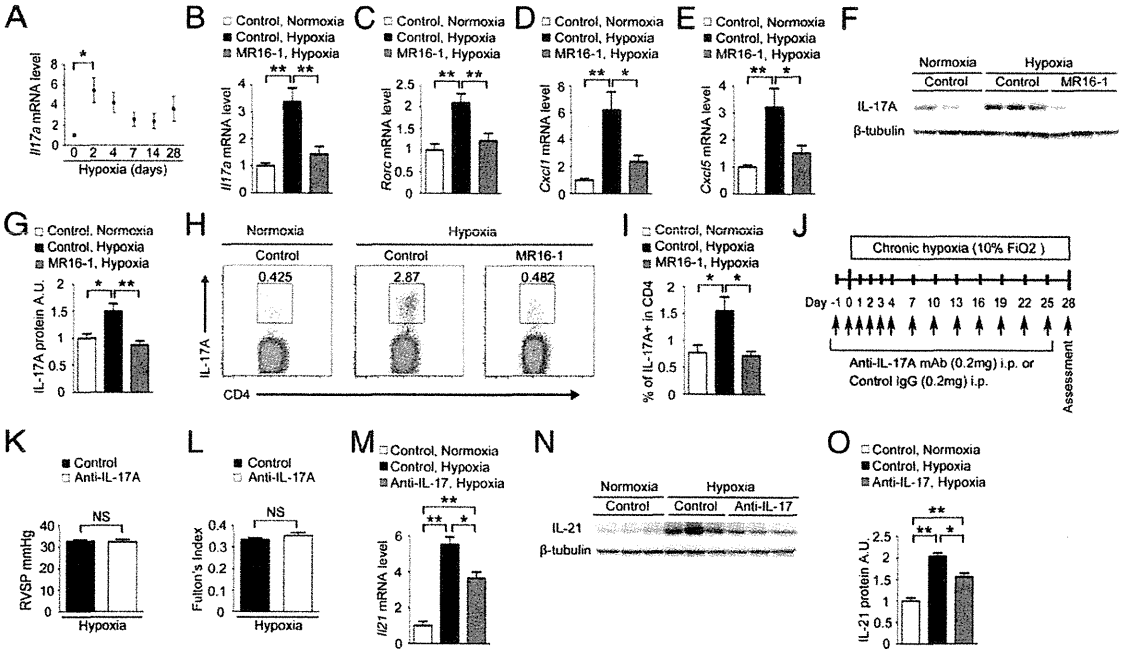


**Fig. 2.** IL-6 blockade inhibits accumulation of Th17 cells in the murine lung after hypoxia exposure. (*A*) qRT-PCR analysis of *Il-17A* mRNA expression in the lungs of C57BL/6 WT mice after hypoxia exposure. The results are pooled data from at least three independent experiments with 5–10 mice per group. (*B–E*) qRT-PCR analysis of *IL-17A* (*B*), *Rorc* (*C*), *Cxcl1* (*D*), and *Cxcl5* (*E*) mRNA expression in the lungs of mice treated with control antibody or MR16-1 after exposure to hypoxia or normoxia for 2 d ($n = 8$). (*F* and *G*) Western blot analysis of IL-17A in the lung homogenates from mice treated with control antibody or MR16-1 after exposure to hypoxia or normoxia for 2 d ($n = 6$). Relative levels of IL-17A protein (normalized to β-tubulin) compared with the normoxic control group are shown. (*H*) Flow cytometric analysis of IL-17A–expressing cells in the $CD4^+$ gated T-cell population isolated from the lungs of mice treated with control antibody or MR16-1 after exposure to hypoxia or normoxia for 3 d ($n = 6$). (*I*) Percentage of $IL\text{-}17A^+$ cells within the $CD4^+$ population. Values shown are the mean ± SEM; $^*P < 0.05$, $^{**}P < 0.01$ calculated using ANOVA. (*J*) Experimental protocol for examining the effect of anti–IL-17A antibody treatment on HPH. An anti–IL-17A neutralizing monoclonal antibody or control antibody (IgG) was administered to C57BL/6 mice under hypoxic conditions. (*K* and *L*) Assessment of antibody-treated mice. RVSP ($n = 6$) (*K*) and Fulton's index ($n = 6$) (*L*) are shown. (*M–O*) IL-17A blockade significantly attenuates the hypoxia-induced IL-21 up-regulation in the murine lungs. (*M*) qRT-PCR analysis of *IL-21* mRNA expression in the lungs of mice treated with control antibody or an anti–IL-17A neutralizing antibody after exposure to hypoxia or normoxia for 2 d ($n = 3$). (*N* and *O*) Western blot analysis of IL-21 in the lung homogenates from mice treated with control antibody or an anti–IL-17A neutralizing antibody after exposure to hypoxia or normoxia for 2 d ($n = 3$). Values shown are the mean ± SEM; $^*P < 0.05$, $^{**}P < 0.01$ calculated using ANOVA. NS, not significant.

treated with control antibody or with MR16-1 exposed to hypoxia (Fig. S1). These findings suggest that IL-6 is critical for the hypoxia-induced accumulation of Th17 cells in the lungs.

We next examined the effect of IL-17 blockade on HPH (Fig. 2*J*). Treatment with an anti–IL-17A neutralizing antibody had no inhibitory effect on the hypoxia-induced elevation in RVSP and Fulton's index compared with control antibody treatment, indicating that IL-17 is not required for HPH development (Fig. 2 *K* and *L*).

**IL-6 Blockade Suppresses the Hypoxia-Induced Accumulation of IL-21–Producing Th17 Cells in the Lungs.** IL-21 is an IL-2 family cytokine produced by activated T cells, including Th17 cells, that regulates immune responses (21). We found that the *Il-21* mRNA level peaked on day 2, remained elevated until day 14, and returned to the basal levels on day 28 after hypoxia exposure (Fig. 3*A*). Hypoxia induced a significantly up-regulated *Il-21* mRNA level in the lungs of mice treated with control antibody but not in the lungs of mice treated with MR16-1 (Fig. 3*B*). Similarly, hypoxia-induced IL-21 protein levels were increased significantly in the lungs of mice treated with control antibody but not in those treated with MR16-1 (Fig. 3 *C* and *D*). In addition, hypoxia induced significantly increased numbers of Th17 cells, which produce both IL-17 and IL-21, in the lungs of mice treated with control antibody but not in those treated with MR16-1 (Fig. 3 *E–G*). These findings suggest that IL-6 promotes the accumulation of IL-21–producing Th17 cells in the lungs after hypoxia exposure.

We also examined the effect of IL-17A blockade with anti–IL-17A neutralizing antibody on the level of IL-21 expression in the lungs after hypoxia exposure. IL-17A blockade significantly attenuated hypoxia-induced up-regulation of IL-21 in the lungs of mice after hypoxia exposure (Fig. 2 *M–O*). These findings suggest that IL-17 is in part involved in the hypoxia-induced up-regulation of IL-21.

**IL-21 Receptor Knockout Mice Are Resistant to HPH.** We next evaluated the effect of hypoxia on IL-21 receptor (IL-21R) knockout (IL-21RKO) mice (Fig. 3*H*) (22). WT mice exposed to hypoxia for 4 wk exhibited significantly increased RVSP, Fulton's index, and medial wall thickness compared with mice exposed to normoxia (Fig. 3 *I–K*). In contrast, the hypoxia-induced elevation of these parameters was inhibited significantly in IL-21RKO mice (Fig. 3 *I–K*). Similarly, remodeling of the medial vascular walls following hypoxia exposure in WT mice also was inhibited significantly in the lungs of IL-21RKO mice (Fig. 3*L*). WT and IL-21RKO mice showed no differences in physiological parameters under normoxia (Table S2). These findings suggest that IL-21R–deficient mice are resistant to HPH.

**IL-6 Blockade Inhibits the Hypoxia-Induced Generation of M2 Macrophages in the Lung.** Alveolar macrophages undergo M2 macrophage polarization in response to hypoxia (19). Therefore, we examined the effect of MR16-1 treatment on the macrophage polarization in the lungs after hypoxia exposure. First, we examined a temporal profile of cell

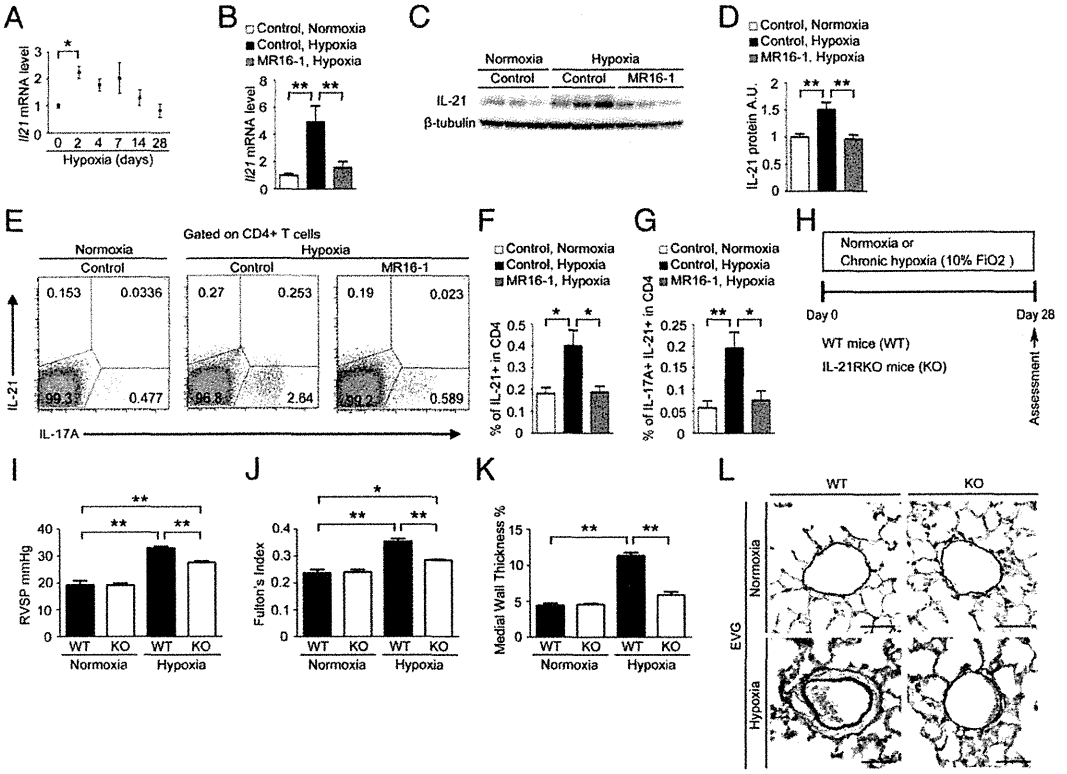


**Fig. 3.** IL-21, a downstream target of IL-6, mediates the development of HPH in mice. (*A*) qRT-PCR analysis of *Il-21* mRNA expression in the lungs of C57BL/6 WT mice after hypoxia exposure. The results are pooled data from at least three independent experiments with 5–10 mice per group. (*B*) qRT-PCR analysis of *IL-21* mRNA expression in the lungs of mice treated with control antibody or MR16-1 after exposure to hypoxia or normoxia for 2 d ($n = 8$). (*C* and *D*) Relative levels of IL-21 protein (normalized to β-tubulin) compared with the normoxic control group. A.U., arbitrary units. (*E*) Flow cytometric analysis of IL-17A$^+$/IL-21$^+$ cells in the CD4$^+$ gated T-cell population isolated from the lungs of mice treated with control antibody or MR16-1 after exposure to hypoxia or normoxia for 3 d ($n = 6$). (*F* and *G*) Percentage of IL-21$^+$ (*F*) and IL-17A$^+$/IL-21$^+$ cells (*G*) within the CD4$^+$ population. (*H*) Experimental protocol for examining the effect of IL-21R deficiency on HPH. (*I–K*) Assessment of WT and IL-21RKO (KO) mice. RVSP ($n = 5$–10) (*I*), Fulton's index ($n = 5$–10) (*J*), and percent wall thickness ($n = 5$) (*K*) are shown. Distal acinar arterioles (50–100 μm in diameter) were examined. (*L*) Representative images of vascular remodeling of the distal acinar arterioles, subjected to elastic Van Gieson staining. (Scale bar: 40 μm.) Values shown are the mean ± SEM; *$P < 0.05$, **$P < 0.01$ calculated using ANOVA.

content in the bronchoalveolar lavage fluid (BALF) of C57BL6 mice after hypoxia exposure. The percentage of the CD45$^+$CD11c$^+$F4/80$^+$ cells in the BALF-isolated living cells was 83.7 ± 0.7% by flow cytometry analysis (Fig. S2 *A* and *B*). The percentage of the alveolar macrophage lineage (CD11c$^+$F4/80$^+$) cells in the CD45$^+$ cells was 92.4 ± 0.9% (Fig. S2*C*). The mRNA levels of *Fizz1* (also known as "*Relmα, resistin-like molecule-α*"), an M2 signature gene, in the alveolar macrophages isolated from the BALF of C57BL6 mice after hypoxia exposure peaked on day 4, were declining on day 7, but remained elevated until day 14 after hypoxia exposure (Fig. 4*A*), indicating that the hypoxia-induced M2 macrophage accumulation in the lung occurred 2 d later than the increase of IL-6 and IL-21 on day 2.

Next, we examined the mRNA levels of *Fizz1* and other M2 signature genes, including *Arg1* (arginase 1), *Chi3l3* (chitinase 3-like 3), *Mrc1* (mannose receptor, C type 1) and *Cxcl12* (also known as "*Sdf1*") in the alveolar macrophages isolated from the BALF after mice were exposed to hypoxia for 4 d. Hypoxia induced significant M2 signature gene up-regulation in the mice treated with control antibody but not in those treated with MR16-1 (Fig. 4 *B–F*). Similarly, hypoxia exposure for 1 wk induced a significant up-regulation of Fizz1 protein levels in the lungs of mice treated with control antibody but not in those of mice treated with MR16-1, as shown by Western blot (Fig. 4 *G* and *H*) and immunohistochemical (Fig. 4 *I* and *J*) analyses. In contrast, there were no significant differences in the mRNA levels of M1 signature genes, including *Nos2* (also known as "*iNos*"), *Il-12β* (*Il-12p40*), and *Tnf-α*, in control- and MR16-1–treated mice following hypoxia exposure (Fig. S3 *A–C*). Notably, treatment with IL-6, soluble IL-6R (sIL-6R), or both IL-6 and sIL-6R had no effect on either M1 or M2 signature gene expression in the alveolar macrophages isolated from BALF (Fig. S4). Collectively, these data indicate that IL-6 indirectly promotes the hypoxia-induced generation of M2 macrophages in the lungs.

**IL-21 Is Indispensable for Hypoxia-Induced M2 Polarization of Alveolar Macrophages in the Lungs.** We hypothesized that IL-21, which has been reported to be majorly secreted from Th17 cells in mice, might play a role in the hypoxia-induced generation of M2 macrophages in the lung. IL-21 treatment of alveolar macrophages isolated from BALF significantly up-regulated the mRNA levels of M2 signature genes, such as *Fizz1*, *Arg1*, and *Cxcl12* (Fig. 5 *A–C*), but had no effect on the mRNA levels of M1 signature genes, including *Nos2*, *Il-12β*, and *Tnf-α* (Fig. S3 *D–F*). These results indicate that IL-21 specifically induces the M2 polarization of alveolar macrophages.

We next examined the effect of IL-21R deletion on the hypoxia-induced up-regulation of M2 signature genes, including *Fizz1*, *Arg1*, and *Cxcl12*, in the alveolar macrophages isolated from the BALF after exposure to hypoxia for 4 d. All these genes were significantly up-regulated in the alveolar macrophages isolated from WT mice but not in those from IL-21RKO mice (Fig. 5 *D–F*). Similarly, Fizz1 protein expression was increased

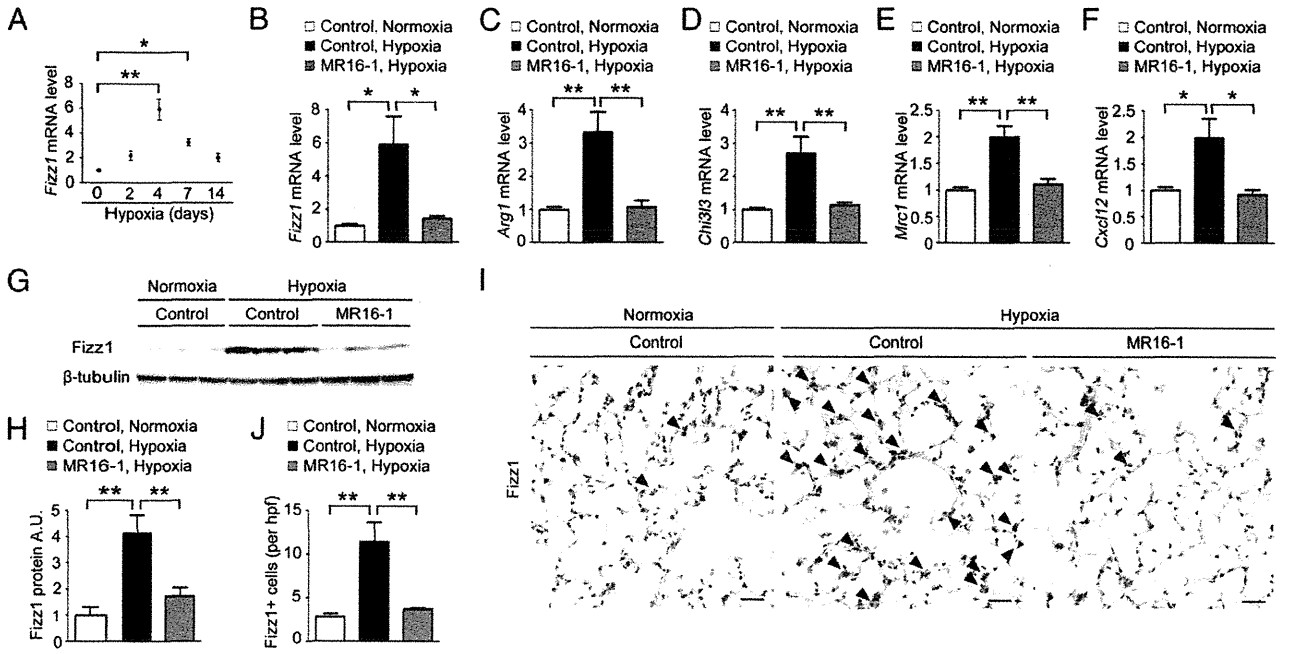


**Fig. 4.** IL-6 blockade ameliorates the hypoxia-induced generation of M2 macrophages in the murine lung. (*A*) qRT-PCR analysis of *Fizz1* mRNA expression in the alveolar macrophages isolated from the BALF of C57BL/6 WT mice after hypoxia exposure. The results are pooled data from three independent experiments with 6 mice per group. (*B–F*) qRT-PCR analysis of M2 macrophage marker genes, including *Fizz1* (*B*), *Arg1* (*C*), *Chi3l3* (*D*), *Mrc1* (*E*), and *Cxcl12* (*F*) in the alveolar macrophages isolated from mice treated with control antibody or MR16-1 after exposure to hypoxia or normoxia for 4 d ($n = 6$). (*G*) Western blot analysis of Fizz1 in lung homogenates from mice treated with control antibody or MR16-1 after exposure to hypoxia or normoxia for 1 wk ($n = 6$). (*H*) Relative Fizz1 protein levels (normalized to β-tubulin level) compared with normoxic mice treated with control antibody. (*I*) Representative Fizz-1 immunostaining of the alveolar areas to detect the accumulation of M2 macrophages (arrowheads) in mice treated with control antibody or MR16-1 after exposure to hypoxia or normoxia for 1 wk ($n = 5$). (Scale bars: 25 μm.) (*J*) Quantification of $Fizz1^+$ cells in the alveolar areas. Data shown are the mean number of positive cells per high-power field ± SEM; $*P < 0.05$, $**P < 0.01$ calculated using ANOVA.

in the lungs of WT mice but not in those of IL-21RKO mice after exposure to hypoxia for 1 wk (Fig. 5 *G* and *H*). In contrast, M1 signature gene expression was comparable in the WT and IL-21RKO mice after exposure to hypoxia (Fig. S3 *G–I*). Consistent with these findings, the hypoxia-induced generation of M2 macrophages in the lung was inhibited significantly by treatment with an anti–IL-21 neutralizing antibody but not by treatment with a control antibody (Fig. 5 *I* and *J*). Collectively, these findings suggest that IL-21 is essential for hypoxia-induced M2 macrophage polarization in the lung.

**IL-21–Induced M2 Macrophage Polarization Is Required for the Hypoxia-Induced Proliferation of PASMCs in the Lung.** We next investigated the molecular mechanism by which the IL-6/IL-21–signaling axis drives the proliferation of PASMCs after hypoxia exposure. Treatment with IL-6, sIL-6R, or both did not promote the proliferation of human PASMCs (HPASMCs), but treatment with FBS (5%) did (Fig. S5*A*). Similarly, treatment with IL-21 did not increase the proliferation of HPASMCs (Fig. S5*B*). Intriguingly, treatment with the conditioned medium of the alveolar macrophages that had been cultivated with IL-21 promoted HPASMC proliferation (Fig. 5*K*), indicating that soluble factors secreted by the M2 macrophages may promote HPASMC proliferation. CXCL12 is a chemokine that stimulates vascular smooth muscle cell proliferation by binding to its receptor CXCR4 (23). Treatment with a selective CXCR4 antagonist, AMD3100, significantly attenuated the proliferative effect of the alveolar macrophage-conditioned medium on the HPASMCs (Fig. 5*L*).

We next examined the effect of IL-21 blockade on the in vivo hypoxia-induced proliferation of PASMCs. Hypoxia exposure significantly increased the number of anti-Ki67 antibody–positive PASMCs in the lungs of WT mice but not in the lungs of IL-21RKO mice (Fig. S5 *C* and *D*). Consistent with this finding, hypoxia exposure significantly increased the number of anti–phospho-histone H3 (p-HH3) antibody–positive PASMCs in the lungs of mice treated with control antibody but not in those treated with the anti–IL-21 neutralizing antibody (Fig. 5 *M* and *N*). Taken together, these data suggest that IL-21 plays a critical role in the hypoxia-induced proliferation of PASMCs in association with M2 macrophage skewing (see Fig. 7).

**Increased Expression of IL-21 and M2 Macrophage Markers in the Lungs of Patients with IPAH.** To validate the clinical significance of our experimental findings, we performed immunohistochemical analyses of the lung tissues from patients with IPAH undergoing lung transplantation. Notably, an excessive infiltration of $IL\text{-}21^+$ cells was detected in the adventitia, obliterative intimal proliferative lesions, and plexiform lesions of the remodeled pulmonary arteries (Fig. 6 *A* and *B*), and more moderate infiltration was detected in the alveolar areas of the lungs of IPAH patients (Fig. 6*C*). In contrast, $IL\text{-}21^+$ cell infiltration was barely detected in the lungs of the control patient (Fig. 6 *A–C*). We also observed both $Arg1^+$ and $MRC\text{-}1^+$ cells in all layers of the remodeled pulmonary arteries and alveolar areas examined in the lungs from patients with IPAH but not in the tissue from control patients (Fig. 6 *D–I*). Together, these findings strongly suggest that the IL-6/IL-21–signaling axis is essential for the pathogenesis of human PAH in association with M2 macrophage polarization (Fig. 7).

## Discussion

Here, we demonstrate that IL-6 blockade by MR16-1 effectively prevented HPH in mice. IL-6 exhibited critical roles in the hypoxia-induced accumulation of Th17 cells and M2 macrophages in the lungs and in the up-regulation of IL-17 and IL-21, which are

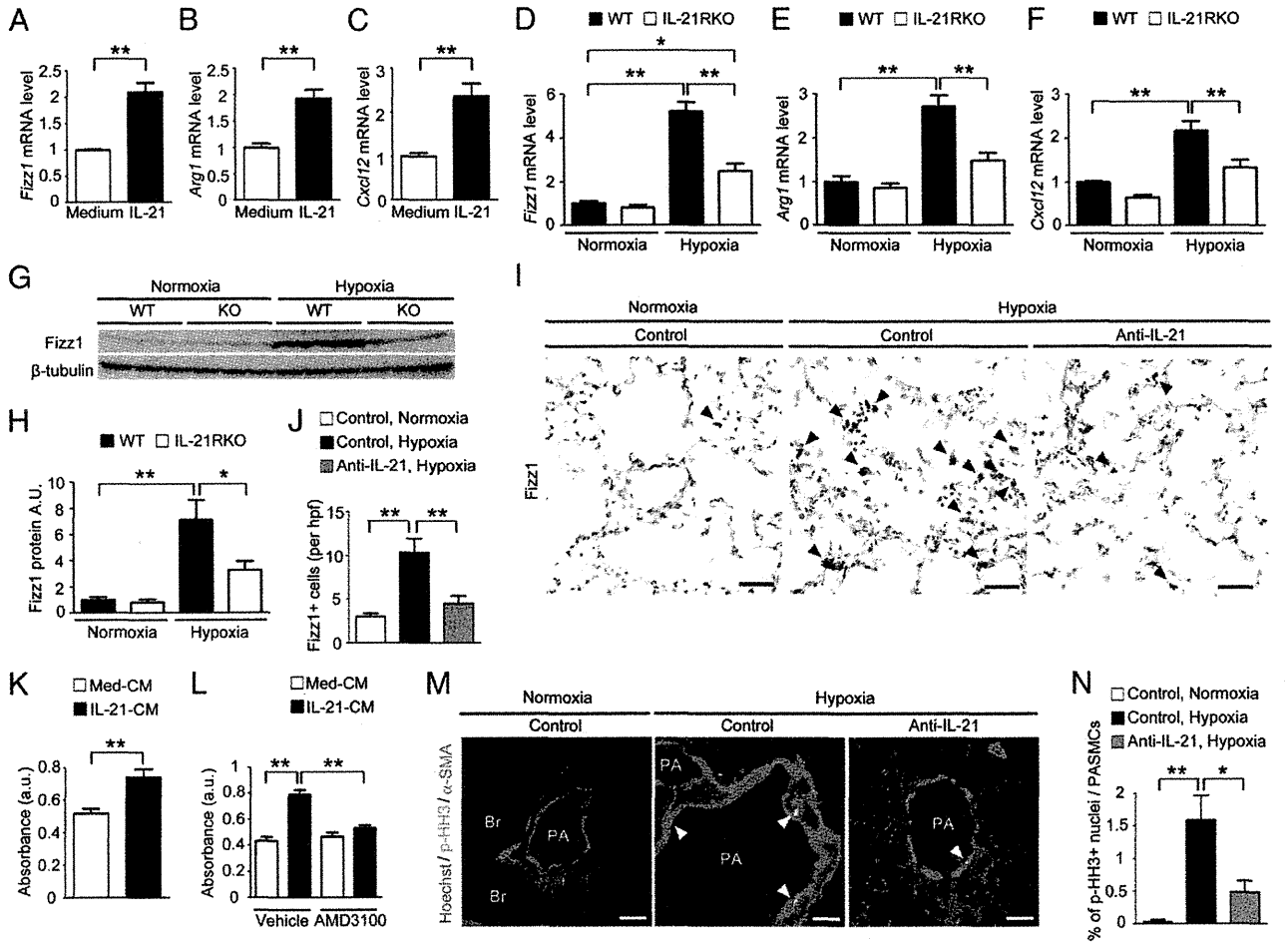


**Fig. 5.** IL-21–induced M2 macrophage polarization is associated with hypoxia-induced pulmonary vascular remodeling. (*A–C*) qRT-PCR analysis of M2 macrophage markers in IL-21–treated primary mouse alveolar macrophages. (*D–F*) qRT-PCR analysis of M2 macrophage markers in alveolar macrophages isolated from WT and IL-21RKO mice after exposure to hypoxia for 4 d ($n = 6$). (*G* and *H*) Fizz1 Western blot analysis of lung homogenates from mice exposed to hypoxia for 1 wk ($n = 6$). (*I*) Fizz1 immunostaining of lung sections from mice treated with control or an anti-IL-21 neutralizing antibody after exposure to hypoxia for 1 wk ($n = 5$). (*J*) Quantification of Fizz1$^+$ cells in the alveolar areas. Values are the mean number of Fizz1$^+$ cells per high-power field ± SEM. (*K*) Effects of the conditioned medium (CM) obtained from primary mouse alveolar macrophages cultivated with IL-21 on the proliferation of HPASMCs. (*L*) Inhibitory effect of AMD3100 on the proliferation of HPASMCs cultured with the conditioned medium of IL-21–treated primary mouse alveolar macrophages. IL-21-CM, conditioned medium of IL-21–treated alveolar macrophages; Med-CM, conditioned medium of control alveolar macrophages. (*M*) p-HH3 (green) and α-smooth muscle actin (α-SMA) (red) immunostaining of lung sections from mice treated with an anti-mouse IL-21 neutralizing antibody after exposure to hypoxia for 1 wk ($n = 5$). (*N*) Percentage of p-HH3$^+$ nuclei (arrowheads) in the PASMCs. (Scale bars: 40 μm.) Br, bronchus; PA, pulmonary artery. Values shown are the mean ± SEM; $^*P < 0.05$, $^{**}P < 0.01$ calculated using ANOVA.

produced mainly by Th17 cells. Although treating mice with a neutralizing IL-17A antibody did not affect HPH development, IL-21R–deficient mice were resistant to HPH and showed no significant accumulation of M2 macrophages in the lungs. Intriguingly, IL-21 was found to promote the M2 polarization of alveolar macrophages in vitro. We also found enhanced expression of IL-21 and M2 macrophage markers in the lung specimens of IPAH patients. Collectively, these findings suggest that the IL-6/IL-21–signaling axis promotes the pathogenesis of PAH, in concert with the accumulation of M2 macrophages in the lungs (Fig. 7).

IL-6 blockade significantly inhibited the Th17-cell accumulation in the lungs after hypoxia exposure (Fig. 2). IL-6, in cooperation with TGF-β, is reported to be critical for the differentiation of Th17 cells from naive CD4$^+$ T cells (15, 24, 25). A humanized monoclonal anti–IL-6R antibody, tocilizumab, is an efficacious therapeutic for patients with rheumatoid arthritis (26, 27). Mechanistically, the protective effect of IL-6 blockade in autoimmune arthritis is attributed primarily to the inhibition of Th17 differentiation (28, 29). Similarly, IL-6 blockade inhibits the induction of Th17 and Th1 cells in an animal model of multiple sclerosis (30). A recent clinical study reported that genes related to IL-17 signaling were up-regulated significantly in lung specimens from patients with IPAH undergoing lung transplantation (31). In addition, previous clinical studies reported that the IL-6 level in the serum or plasma correlated with the severity of pulmonary hypertension in the patients with IPAH and chronic obstructive pulmonary disease (9, 10, 32). Collectively, these findings indicate that the IL-6/Th17–signaling axis plays a key role in the pathogenesis of inflammatory diseases, including PAH.

IL-6 blockade by MR16-1 also abrogated the hypoxia-induced M2 macrophage polarization in the lungs (Fig. 4). M2 macrophage polarization has been implicated in the pathogenesis of pulmonary hypertension (19, 33, 34), and immunization with certain antigens evokes pulmonary arterial muscularization along with a Th2 response and the subsequent polarization of M2 macrophages (33). Notably, the lung-specific transgenic overexpression of heme oxygenase-1 effectively inhibits the hypoxia-induced up-regulation of inflammatory cytokines (including IL-6), M2 macrophage

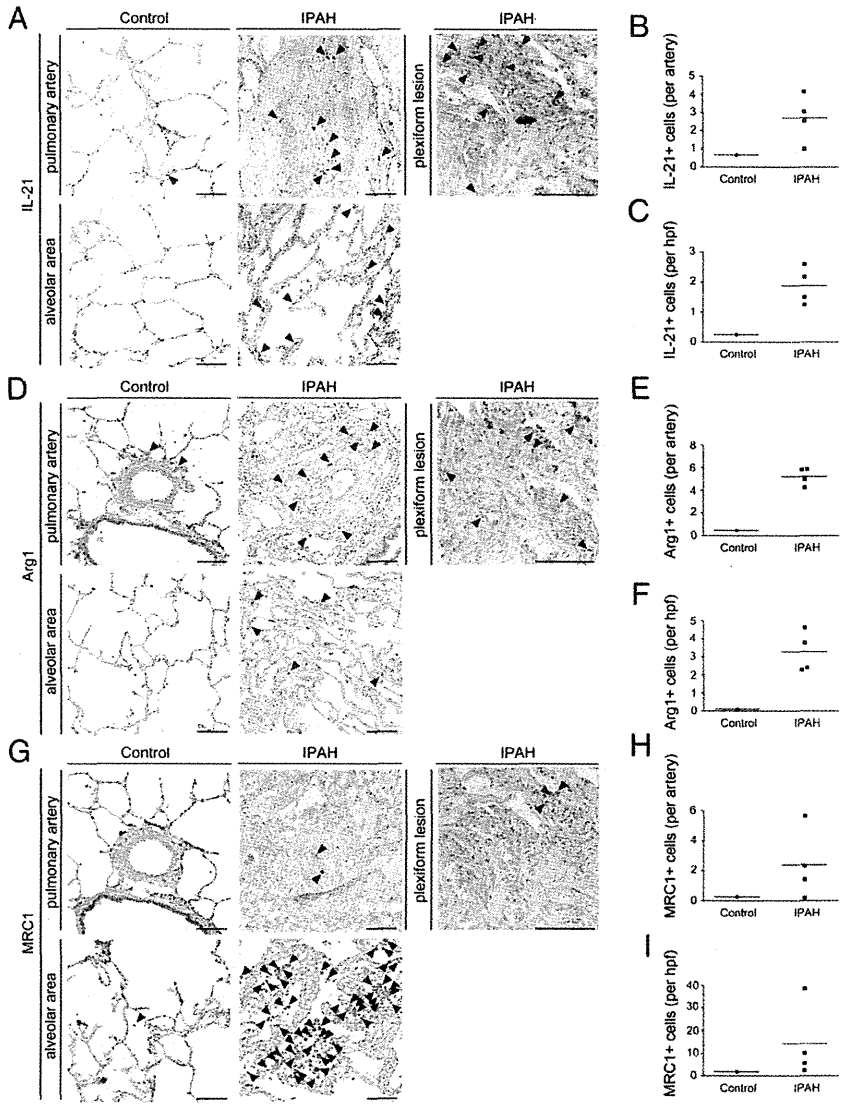


**Fig. 6.** Significantly enhanced expression of IL-21 and M2 macrophage markers is detected in the lungs of IPAH patients who underwent lung transplantation. (*A*, *D*, and *G*) Representative IL-21, Arg1, and MRC-1 immunostaining of the pulmonary artery, plexiform lesion, and alveolar area from the lungs of a control patient and patients with IPAH. Arrowheads indicate IL-21$^+$ (*A*), Arg1$^+$ (*D*), and MRC-1$^+$ (*G*) cells. (Scale bars: 100 μm.) (*B*, *E*, and *H*) The numbers of IL-21$^+$ (*B*), Arg1$^+$ (*E*), and MRC-1$^+$ (*H*) cells around one pulmonary artery of a control patient and IPAH patients. The horizontal line in the graph indicates the mean number in each group. (*C*, *F*, and *I*) The numbers of IL-21$^+$ (*C*), Arg1$^+$ (*F*), and MRC-1$^+$ (*I*) cells per high-power field in the alveolar areas of the control patient and IPAH patients. The horizontal line in the graph indicates the mean number in each group.

accumulation, and the subsequent development of pulmonary hypertension (19, 34). Taken together, these data suggest that IL-6 blockade may prevent HPH, at least in part, by inhibiting M2 macrophage polarization.

IL-6 is reported to induce the up-regulation of IL-21 in naive and memory CD4$^+$ T cells (35, 36). In addition, IL-21 also is produced by Th17 cells and drives Th17 differentiation in an autocrine manner (36–38). Here we found that hypoxia exposure induced transient expression of IL-6 and prolonged expression of IL-17 and IL-21 in the lungs (Figs. 1*A*, 2*A*, and 3*A*). The prolonged induction of IL-17 and IL-21 may result from the autocrine production of IL-21 by Th17 cells. Taken together, these findings indicate that IL-21 may be critical for the sustained inflammation that promotes the development of pulmonary hypertension.

The involvement of IL-21 in M2 macrophage polarization has been reported previously (39, 40). In a colitis-associated colon cancer model, IL-21RKO mice show less M2 macrophage infiltration into tumors than WT model mice (40). IL-21RKO mice also exhibit a markedly reduced expression of several M2 macrophage-related genes in the lungs when infected with parasites, as compared with WT mice (40). Here, we found that IL-21RKO mice were resistant to HPH and failed to accumulate M2 macrophages in the lungs after hypoxia exposure, unlike WT mice (Figs. 3 *H–L* and 5 *D–F*). Furthermore, we found that the expression levels of IL-21 and of M2 macrophage signature genes were up-regulated in the lungs of IPAH patients (Fig. 6). This last finding supports the clinical significance of the link between the IL-6/IL-21–signaling axis and the pathogenesis of PAH suggested by the results of our animal studies.

In conclusion, our findings indicate that the IL-6/IL-21–signaling axis plays a critical role in the pathogenesis of PAH and suggest that this signaling axis may yield potential therapeutic targets for treating patients with PAH.

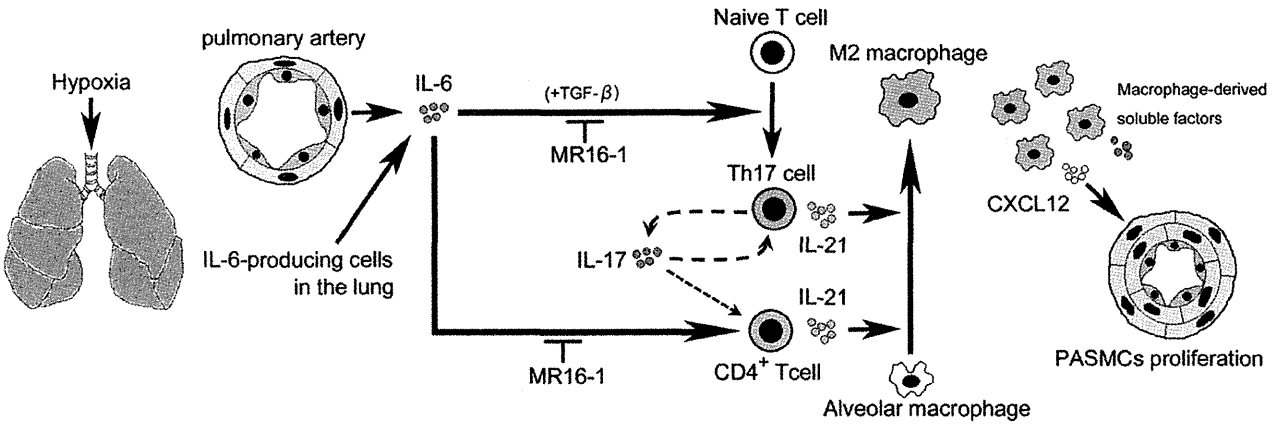


**Fig. 7.** Schematic illustration of the development of PAH through the IL-6/Th17/IL-21–signaling axis. Hypoxia induces the up-regulation of IL-6 in the PAECs (orange) and PASMCs (yellow). IL-6 promotes the differentiation of Th17 cells from naive T cells, presumably in cooperation with TGF-β in the lung. IL-17, derived mainly from Th17 cells, is partly responsible for the production of IL-21 in these cells. IL-21, secreted from $CD4^+$ T cells, including Th17 cells, promotes macrophage skewing toward the M2 phenotype in the alveolar macrophages. M2 macrophages positively regulate the hypoxia-induced proliferation of PASMCs by releasing soluble factors such as CXCL12. Taken together, these data show that IL-21 plays a critical role in the pathogenesis of PAH in concert with M2 macrophage polarization downstream of the IL-6/IL-21–signaling axis and may be a potential therapeutic target for treating patients with PAH.

## Materials and Methods

Full experimental procedures and associated references are available in *SI Materials and Methods*.

**Animals.** All experiments were carried out under the guidelines of the Osaka University Committee for Animal and Recombinant DNA Experiments and the local Animal Ethics Committee of the National Cerebral and Cardiovascular Center Research Institute (Osaka) and also were approved by the Institutional Review Board of Osaka University and the National Cerebral and Cardiovascular Center Research Institute. Male C57BL/6 8-wk-old mice (average body weight: 21.4 g) purchased from Japan SLC, Inc. were used in the experiments. In most of the experiments examining the effect of IL-6 blockade, the mice were divided into four groups: normoxic control antibody group ($n = 8$), normoxic MR16-1 group ($n = 8$), hypoxic control antibody group ($n = 10$), and hypoxic MR16-1 group ($n = 12$). IL-21RKO mice were kindly provided by Warren J. Leonard, National, Heart, Lung, and Blood Institute, Bethesda (22). IL-21RKO heterozygous mice were intercrossed, and male 8-wk-old littermates of WT and IL-21RKO mice were used in the following experiments. The average body weight of the male IL-21RKO mice was 21.5 g. In most of the experiments examining the effect of IL-21R deficiency, the mice were divided into four groups: normoxic WT group ($n = 5$), normoxic IL-21RKO group ($n = 5$), hypoxic WT group ($n = 10$), and hypoxic IL-21RKO group ($n = 9$). All mice were housed on a 12-h light/12-h dark cycle at 24 ± 1 °C and were given standard mouse food and water ad libitum. The mice either were housed under standard normoxic conditions or were housed continuously in a hypoxic chamber (10% $O_2$) for up to 4 wk, except for a 5-min interval twice a week when the chamber was cleaned. The hypoxic gas mixture was delivered continuously to the chamber at a flow rate of ~1 L/min. After chronic hypoxic exposure, the mice were subjected to hemodynamic recording and were killed for pathological analysis of the heart and lungs.

**Treatment of Mice with Neutralizing Antibodies.** MR16-1, a rat IgG1 monoclonal neutralizing antibody against murine IL-6R, was kindly provided by Chugai Pharmaceutical Co. (41). To determine the effect of the MR16-1–mediated blockade of IL-6, mice were i.v. injected with 2 mg of MR16-1 or purified rat nonimmune isotype control IgG (MP Biomedicals) just before exposure to hypoxia or normoxia and subsequently were injected i.p. with 0.5 mg of MR16-1 or control IgG, respectively, once a week. To block IL-17A, mice were injected i.p. with 200 μg of a neutralizing anti–mouse IL-17A monoclonal antibody, MAB421 (R&D Systems) or isotype control IgG on days −1, 0, 1, 2, 3, 4, 7, 10, 13, 16, 19, 22, and 25 after hypoxia exposure was initiated. To block IL-21, mice were injected i.p. with 100 μg of a neutralizing anti–mouse IL-21 monoclonal antibody (FFA21; eBioscience) or isotype control IgG on days −1, 0, 1, 2, 3, and 4 after exposure to hypoxia or normoxia was initiated.

**Surgical Preparation and Blood Pressure Measurements.** Mice were anesthetized with pentobarbital sodium (60 mg/kg i.p.) and an analgesic agent, butorphanol tartrate (0.1–0.4 mg/kg i.p.). Supplementary doses of pentobarbital (15–20 $mg \cdot kg^{-1} \cdot h^{-1}$ i.p.) and butorphanol tartrate (0.03–0.05 $mg \cdot kg^{-1} \cdot h^{-1}$ i.p.) were administered periodically to maintain a surgical level of anesthesia. Throughout the procedure, the body temperature was maintained at 37–38 °C using a rectal thermistor coupled with a thermostatically controlled heating pad. The trachea was cannulated, and the lungs were ventilated with a mouse ventilator (Minivent Type 845; Harvard Apparatus) (42). The inspirated gas was enriched with oxygen, and the ventilator settings were adjusted (tidal volume 6 μL/g; frequency ~170–190/min). A polyethylene tube was inserted into the right external jugular vein and advanced into the right ventricle (RV) to measure right ventricular pressure (RVP). RVP signals were detected by a pressure transducer (MLT0670; AD Instruments), and the signals were relayed to pressure amplifiers (ML117; AD Instruments) and then were sampled continuously with a PowerLab system (AD Instruments) and recorded on a computer using Chart software (AD Instruments) (42). Heart rate (HR) was derived from the right ventricular systolic peaks and was typically between 300 and 500 beats/min (bpm) under these conditions. If the HR fell below 300 bpm, the measurements were excluded from the analysis. Systemic arterial blood pressure was obtained noninvasively from conscious mice using a computerized tail-cuff system (BP-98A-L; Softron) as described previously (43).

**Western Blot Analysis.** Frozen lungs were homogenized in 50 mM Hepes, 100 mM sodium fluoride, 2 mM sodium orthovanadate, 4 mM EDTA, 1% Tween-20, 0.1% SDS, and Complete protease inhibitor mixture (Roche Applied Science) using a Polytron homogenizer (PT 10-35GT; Kinematica) as described previously (44). The precleared lysates then were resolved by SDS/PAGE and subjected to Western blot analysis using a standard procedure with the following antibodies: anti–pSTAT3-Tyr705 (clone D3A7; Cell Signaling), anti-STAT3 (clone 79D7; Cell Signaling), anti-RELM alpha (Fizz1) (ab39626; Abcam), anti–IL-17A (sc-52567; Santa Cruz), and anti–IL-21 (MAB594; R&D Systems). An anti–β-tubulin antibody (T5201; Sigma-Aldrich) was used as the internal control. The blots were developed using HRP-coupled secondary antibodies (Cell Signaling Technology) and the ECL system (GE Healthcare).

**Morphometric Analysis.** After hemodynamic recording, the mice were killed by anesthesia overdose, and the heart was excised. The atria were removed, and the RV wall was separated from the left ventricle (LV) and septum. The tissues were blotted, weighed, and their weights normalized to a 100-g body weight. Fulton's index, the ratio of RV to LV + septum weight [RV/(LV + S)] was used as an index of right ventricular hypertrophy (45). The lungs then were harvested for histological and immunohistochemical analyses. The pulmonary artery and trachea were perfused with 4% (wt/vol) paraformaldehyde (PFA) at constant pressure (100 cm $H_2O$ for the pulmonary artery and 25 cm $H_2O$ for the trachea) to distend fully the pulmonary blood vessels and airway, respectively. Excised lungs were fixed in 4% PFA overnight at 4 °C and then were embedded in paraffin and cut into 4-μm-thick sections. For pulmonary

vascular morphometry, paraffin-embedded lung sections were subjected to elastic Van Gieson staining. Images of arteries were captured with a fluorescence microscope (BZ-9000; Keyence). Morphometry was performed on lung sections obtained from five or six randomly chosen animals in each treatment group. Pulmonary remodeling was assessed by the percent wall thickness of parenchymal pulmonary arteries classified into the small arteries (terminal bronchioles) and arterioles (acini or alveolar ducts). The percent wall thickness was the medial wall thickness (the distance between the internal and external lamina) × 2 divided by the diameter of the vessel (the distance between the external lamina) × 100. For vessels with a single elastic lamina, the distance between the elastic and endothelial basement membrane was measured. Medial thickness was analyzed only for sectioned vessels exhibiting an approximately circular profile. The diameter of pulmonary arteries was determined by Image J software (National Institutes of Health). The percent wall thickness was calculated for at least 10 small pulmonary arteries and arterioles for each mouse.

**Lung Specimens from Patients with IPAH.** All the experiments using human specimens were approved by the Institutional Review Board of Osaka University, Suita, Japan. The lung tissues were obtained from four patients with IPAH undergoing lung transplantation and from a control patient undergoing surgery for lung cancer at a site far away from the tumor margins. All lung specimens were procured at Osaka University Hospital. Before surgery, all patients provided written consent for the use of their lung tissues for biomedical research. The resected lung tissues were fixed in 10% PFA. Patient characteristics are shown in Table S3.

**Histological and Immunohistochemical Analyses of the Pulmonary Vasculatures.** For the immunohistochemical analyses of murine lung tissues, samples were fixed in 4% PFA/PBS for 1 h, cryoprotected with PBS containing 5–20% sucrose, frozen in OCT compound (Sakura), and cut into 10-μm-thick cryosections as described previously (46). Human lung samples, which were formaldehyde-fixed and paraffin-embedded, were cut into 5-μm-thick sections, deparaffinized, and rehydrated. The human sections were subjected to antigen retrieval either by heat induction in 10 mM sodium citrate buffer, pH 6.0, or by proteinase K digestion for 3 min. All lung sections then were washed in PBS, treated with 1% hydrogen peroxide in methanol for 30 min, incubated in blocking solution containing either 1% BSA or 5% skim milk in PBS and 0.1% Triton-X (PBST) for 1 h, and incubated with primary antibody in PBST overnight at 4 °C or 25 °C. The following primary antibodies were used for immunostaining: anti-RELM alpha (Fizz1) (1:100 dilution; ab39626; Abcam); anti–IL-6 (1:200 dilution; ab6672; Abcam); anti- p-HH3 (Ser10) (1:100 dilution; 06–570; Upstate); anti-Ki67 (1:200 dilution; ab16667; Abcam); anti-Actin, alpha-Smooth Muscle-Cy3 (1:200 dilution; C6198; Sigma-Aldrich); anti-Arg1 (1:1,000 dilution; HPA024006; Sigma-Aldrich); anti-mannose receptor (MRC1) (1:1,000 dilution; ab64693; Abcam); and anti–IL-21 (1:200 dilution; NBP1-02706; Novus). Next, the sections were washed in PBST and incubated with fluorescence-conjugated (1:200 dilution; Alexa Fluor 488- or 546-coupled; Invitrogen) or HRP-coupled (1:200 or 1:400 dilution; 7074; Cell Signaling Technology) secondary antibodies for 1 h at room temperature, and, if necessary, were visualized using 3,3′-diaminobenzidine substrate (Sigma). Images were acquired with a fluorescence microscope (BZ-9000; Keyence). Negative control sections for the immunohistochemical experiments received identical treatment except for exposure to the primary antibodies and showed no specific staining. $Fizz1^+$ cells were counted in 10–20 high-power fields (magnification: 400×) per mouse. $p\text{-}HH3^+$ cells and $Ki67^+$ cells were counted in at least 10 pulmonary arteries for each mouse. $Arg1^+$, $MRC1^+$, and $IL\text{-}21^+$ cells were counted in at least 10 pulmonary arteries or at least 10 high-power fields (magnification: 200×) in the alveolar area from each human sample.

**Flow Cytometry Analysis.** Lung tissue was incubated directly for 40 min to 1 h at 37 °C in DMEM containing collagenase and DNase1 (1 U/mL) (Takara). The tissue suspensions then were pressed through a 40-μm mesh, pelleted, resuspended in PBS-F (PBS containing 2% FBS), and the cells were washed twice with PBS-F. The cells were preincubated with an antibody to CD16/32 to block Fcγ receptors and then were washed and incubated with the indicated fluorophore-conjugated antibody (CD4) for 30 min in a total volume of 100 μL PBS-F. For intracellular cytokine staining, the cells first were stimulated for 5 h in complete medium in the presence of 25 ng/mL phorbol12-myristate13-acetate, 1 μg/mL ionomycin, and 10 μg brefeldin A (Sigma-Aldrich) and then were stained for CD4, followed by fixation and permeabilization using the Mouse Foxp3 Buffer Set (BD Pharmingen) according to the manufacturer's instructions. After two washes, the cells were stained for 30 min on ice with fluorophore-conjugated antibodies (anti–IFN-γ, anti–IL-4, anti–IL-17A, anti–IL-21) or the appropriate isotype control antibodies. The purity of the cells isolated from BALF was assessed by using the fluorophore-conjugated antibodies against CD45, F4/80, and CD11c or the appropriate isotype control antibodies. Dead cells were excluded by propidium iodide. The cells then were analyzed on a FACSCanto (BD Biosciences), followed by analysis with FlowJo software (Tri-Star). The following antibodies were used for flow cytometry analyses: FITC-conjugated anti-CD4 (RM4-5), PE-conjugated anti–IFN-γ (XMG1.2), APC-conjugated anti–IL-4 (11B11), APC-conjugated anti–IL-17A (eBio17B7), PE-conjugated anti–IL-21 (mhalx21), and APC-conjugated anti-F4/80 (BM8) from eBioscience and PE-conjugated anti-CD45 (30-F11) and FITC-conjugated anti-CD11c (HL3) from BD Biosciences.

**qRT-PCR.** Total RNA from the mouse lung or alveolar macrophages was extracted using TRIzol reagent (Invitrogen). qRT-PCR was carried out using the QuantiFast SYBRGreen RT-PCR kit (Qiagen) as described previously (47). For each reaction, 80 ng of total RNA was transcribed for 10 min at 50 °C, followed by a denaturing step at 95 °C for 5 min and 40 cycles of 10 s at 95 °C and 30 s at 60 °C. Fluorescence data were collected and analyzed using an ABI PRISM 7900HT. The following primers were used: *Gapdh*: 5′-TCTCCACACCTATGGTGCAA-3′, 5′-CAAGAAACAGGGGAGCTGAG-3′; *Fizz1*: 5′-CCCTTCTCATCTGCATCTCC-3′, 5′-AGGAGGCCCATCTGTTCATA-3′; *Arg1*: 5′-GTGAAGAACCCACGGTCTGT-3′, 5′-CTGGTTGTCAGGGGAGTGTT-3′; *Chi3l3*: 5′-CCCACCAGGAAAGTACACAG-3′, 5′-GAGGGAAATGTCTCTGGTGA-3′; *Mrc1*: 5′-CGCGAGGCAATTTTTAATCT-3′, 5′-ATTTGCATTGCCCAGTAAGG-3′; *Cxcl12*: 5′-GGTTCTTCGAGAGCCACATC-3′, 5′-TAATTTCGGGTCAATGCACA-3′; *Il17a*: 5′-TCCAGAAGGCCCTCAGACTA-3′, 5′-CTCGACCCTGAAAGTGAAGG-3′; *Rorc*: 5′-AACCAGGCATCCTGAACTTG-3′, 5′-CGTAGAAGGTCCTCCAGTCG-3′; *Cxcl1*: 5′-GCCTATCGCCAATGAGCTG-3′, 5′-TCTGAACCAAGGGAGCTTCA-3′; *Cxcl5*: 5′-CTGCCCCTTCCTCAGTCATA-3′, 5′-TGGATCCAGACAGACCTCCT-3′; *Il21*: 5′-GGACAGTGGCCCATAAATCA -3′, 5′- CAGGGTTTGATGGCTTGAGT -3′; *Il6*: 5′- TGTGCAATGGCAATTCTGAT-3′, 5′-GGTACTCCAGAAGACCAGAGGA-3′; *Nos2*: 5′-GCTCATGACATCGACCAGAA-3′, 5′-TGTTGCATTGGAAGTGAAGC-3′; *Il12b*: 5′-AGGTCACACTGGACCAAAGG-3′, 5′-AGGGTACTCCCAGCTGACCT-3′; *Tnf-α*: 5′-TGCCTATGTCTCAGCCTCTTC-3′, 5′-GGTCTGGGCCATAGAACTGA-3′.

**Statistics.** All data are expressed as the mean ± SEM. Differences among multiple groups were compared by one-way ANOVA followed by a post hoc comparison tested with Scheffé's method. The Student's *t* test was used to analyze differences between two groups. $P < 0.05$ was considered statistically significant.

**ACKNOWLEDGMENTS.** We thank Yuka Yoshimoto and Yumi Yanagisawa for secretarial assistance; Kaori Yamamoto and Manami Sone (National Cerebral and Cardiovascular Research Center) for technical assistance; Yoshito Takeda, Yingji Jin (Osaka University), Yasunobu Arima (Hokkaido University), Hatsue Ueda, Naoki Mochizuki (National Cerebral Cardiovascular Research Center), Susumu Nakae, and Tomokazu Sumida (University of Tokyo) for helpful discussions and suggestions; Warren J. Leonard (National, Heart, Lung, and Blood Institute) for providing IL-21RKO mice; and Chugai Pharmaceutical Co. for providing the anti–IL-6R antibody MR16-1. This work was supported in part by Grant KAKENHI-25670386 from the Ministry of Education, Science, Sports and Culture of Japan (to Y.N.) and by a grant from Precursory Research for Embryonic Science and Technology, Japan Science Technology Agency (to Y.N.).

1. Pietra GG, et al. (2004) Pathologic assessment of vasculopathies in pulmonary hypertension. *J Am Coll Cardiol* 43(12, Suppl S):25S–32S.
2. Rabinovitch M (2012) Molecular pathogenesis of pulmonary arterial hypertension. *J Clin Invest* 122(12):4306–4313.
3. Dorfmüller P, Perros F, Balabanian K, Humbert M (2003) Inflammation in pulmonary arterial hypertension. *Eur Respir J* 22(2):358–363.
4. Schermuly RT, Ghofrani HA, Wilkins MR, Grimminger F (2011) Mechanisms of disease: Pulmonary arterial hypertension. *Nat Rev Cardiol* 8(8):443–455.
5. Tuder RM, Groves B, Badesch DB, Voelkel NF (1994) Exuberant endothelial cell growth and elements of inflammation are present in plexiform lesions of pulmonary hypertension. *Am J Pathol* 144(2):275–285.
6. Tuder RM, Voelkel NF (1998) Pulmonary hypertension and inflammation. *J Lab Clin Med* 132(1):16–24.
7. Kishimoto T (2006) Interleukin-6: Discovery of a pleiotropic cytokine. *Arthritis Res Ther* 8(Suppl 2):S2.
8. Kishimoto T, Akira S, Taga T (1992) Interleukin-6 and its receptor: A paradigm for cytokines. *Science* 258(5082):593–597.
9. Humbert M, et al. (1995) Increased interleukin-1 and interleukin-6 serum concentrations in severe primary pulmonary hypertension. *Am J Respir Crit Care Med* 151(5): 1628–1631.
10. Soon E, et al. (2010) Elevated levels of inflammatory cytokines predict survival in idiopathic and familial pulmonary arterial hypertension. *Circulation* 122(9):920–927.

11. Steiner MK, et al. (2009) Interleukin-6 overexpression induces pulmonary hypertension. *Circ Res* 104(2):236–244.
12. Savale L, et al. (2009) Impact of interleukin-6 on hypoxia-induced pulmonary hypertension and lung inflammation in mice. *Respir Res* 10:6.
13. Iwakura Y, Ishigame H, Saijo S, Nakae S (2011) Functional specialization of interleukin-17 family members. *Immunity* 34(2):149–162.
14. Korn T, Bettelli E, Oukka M, Kuchroo VK (2009) IL-17 and Th17 Cells. *Annu Rev Immunol* 27:485–517.
15. Bettelli E, et al. (2006) Reciprocal developmental pathways for the generation of pathogenic effector TH17 and regulatory T cells. *Nature* 441(7090):235–238.
16. Biswas SK, Mantovani A (2010) Macrophage plasticity and interaction with lymphocyte subsets: Cancer as a paradigm. *Nat Immunol* 11(10):889–896.
17. Mosser DM, Edwards JP (2008) Exploring the full spectrum of macrophage activation. *Nat Rev Immunol* 8(12):958–969.
18. Wynn TA, Chawla A, Pollard JW (2013) Macrophage biology in development, homeostasis and disease. *Nature* 496(7446):445–455.
19. Vergadi E, et al. (2011) Early macrophage recruitment and alternative activation are critical for the later development of hypoxia-induced pulmonary hypertension. *Circulation* 123(18):1986–1995.
20. Tanaka T, Narazaki M, Kishimoto T (2012) Therapeutic targeting of the interleukin-6 receptor. *Annu Rev Pharmacol Toxicol* 52:199–219.
21. Liu SM, King C (2013) IL-21-producing Th cells in immunity and autoimmunity. *J Immunol* 191(7):3501–3506.
22. Ozaki K, et al. (2002) A critical role for IL-21 in regulating immunoglobulin production. *Science* 298(5598):1630–1634.
23. Takeda Y, et al. (2011) Macrophage skewing by Phd2 haplodeficiency prevents ischaemia by inducing arteriogenesis. *Nature* 479(7371):122–126.
24. Mangan PR, et al. (2006) Transforming growth factor-beta induces development of the T(H)17 lineage. *Nature* 441(7090):231–234.
25. Veldhoen M, Hocking RJ, Atkins CJ, Locksley RM, Stockinger B (2006) TGFbeta in the context of an inflammatory cytokine milieu supports de novo differentiation of IL-17-producing T cells. *Immunity* 24(2):179–189.
26. Choy EH, et al. (2002) Therapeutic benefit of blocking interleukin-6 activity with an anti-interleukin-6 receptor monoclonal antibody in rheumatoid arthritis: A randomized, double-blind, placebo-controlled, dose-escalation trial. *Arthritis Rheum* 46(12): 3143–3150.
27. Nishimoto N, et al. (2004) Treatment of rheumatoid arthritis with humanized anti-interleukin-6 receptor antibody: A multicenter, double-blind, placebo-controlled trial. *Arthritis Rheum* 50(6):1761–1769.
28. Fujimoto M, et al. (2008) Interleukin-6 blockade suppresses autoimmune arthritis in mice by the inhibition of inflammatory Th17 responses. *Arthritis Rheum* 58(12):3710–3719.
29. Iwanami K, et al. (2008) Crucial role of the interleukin-6/interleukin-17 cytokine axis in the induction of arthritis by glucose-6-phosphate isomerase. *Arthritis Rheum* 58(3): 754–763.
30. Serada S, et al. (2008) IL-6 blockade inhibits the induction of myelin antigen-specific Th17 cells and Th1 cells in experimental autoimmune encephalomyelitis. *Proc Natl Acad Sci USA* 105(26):9041–9046.
31. Hsu E, et al. (2011) Lung tissues in patients with systemic sclerosis have gene expression patterns unique to pulmonary fibrosis and pulmonary hypertension. *Arthritis Rheum* 63(3):783–794.
32. Chaouat A, et al. (2009) Role for interleukin-6 in COPD-related pulmonary hypertension. *Chest* 136(3):678–687.
33. Daley E, et al. (2008) Pulmonary arterial remodeling induced by a Th2 immune response. *J Exp Med* 205(2):361–372.
34. Minamino T, et al. (2001) Targeted expression of heme oxygenase-1 prevents the pulmonary inflammatory and vascular responses to hypoxia. *Proc Natl Acad Sci USA* 98(15):8798–8803.
35. Dienz O, et al. (2009) The induction of antibody production by IL-6 is indirectly mediated by IL-21 produced by CD4+ T cells. *J Exp Med* 206(1):69–78.
36. Nurieva R, et al. (2007) Essential autocrine regulation by IL-21 in the generation of inflammatory T cells. *Nature* 448(7152):480–483.
37. Korn T, et al. (2007) IL-21 initiates an alternative pathway to induce proinflammatory T(H)17 cells. *Nature* 448(7152):484–487.
38. Zhou L, et al. (2007) IL-6 programs T(H)-17 cell differentiation by promoting sequential engagement of the IL-21 and IL-23 pathways. *Nat Immunol* 8(9):967–974.
39. Pesce J, et al. (2006) The IL-21 receptor augments Th2 effector function and alternative macrophage activation. *J Clin Invest* 116(7):2044–2055.
40. Stolfi C, et al. (2011) Involvement of interleukin-21 in the regulation of colitis-associated colon cancer. *J Exp Med* 208(11):2279–2290.
41. Takagi N, et al. (1998) Blockage of interleukin-6 receptor ameliorates joint disease in murine collagen-induced arthritis. *Arthritis Rheum* 41(12):2117–2121.
42. Sonobe T, et al. (2011) Imaging of the closed-chest mouse pulmonary circulation using synchrotron radiation microangiography. *J Appl Physiol (1985)* 111(1):75–80.
43. Higuchi K, et al. (2012) Endothelial Gab1 deletion accelerates angiotensin II-dependent vascular inflammation and atherosclerosis in apolipoprotein E knockout mice. *Circ J* 76(8):2031–2040.
44. Nakaoka Y, et al. (2007) Gab family proteins are essential for postnatal maintenance of cardiac function via neuregulin-1/ErbB signaling. *J Clin Invest* 117(7): 1771–1781.
45. Ogura S, et al. (2013) Oxidative stress augments pulmonary hypertension in chronically hypoxic mice overexpressing the oxidized LDL receptor. *Am J Physiol Heart Circ Physiol* 305(2):H155–H162.
46. Arita Y, et al. (2014) Myocardium-derived angiopoietin-1 is essential for coronary vein formation in the developing heart. *Nat Commun* 5:4552.
47. Shioyama W, et al. (2011) Docking protein Gab1 is an essential component of postnatal angiogenesis after ischemia via HGF/c-met signaling. *Circ Res* 108(6):664–675.

ARTHRITIS & RHEUMATOLOGY
Vol. 67, No. 6, June 2015, pp 1481–1490
DOI 10.1002/art.39086
© 2015 The Authors. Arthritis & Rheumatology is published by Wiley Periodicals, Inc. on behalf of the American College of Rheumatology. This is an open access article under the terms of the Creative Commons Attribution-NonCommercial-NoDerivs License, which permits use and distribution in any medium, provided the original work is properly cited, the use is non-commercial and no modifications or adaptations are made.

# Semaphorin 4D Contributes to Rheumatoid Arthritis by Inducing Inflammatory Cytokine Production

## Pathogenic and Therapeutic Implications

Yuji Yoshida,[1] Atsushi Ogata,[1] Sujin Kang,[1] Kousuke Ebina,[1] Kenrin Shi,[2] Satoshi Nojima,[1] Tetsuya Kimura,[1] Daisuke Ito,[1] Keiko Morimoto,[1] Masayuki Nishide,[1] Takashi Hosokawa,[1] Toru Hirano,[1] Yoshihito Shima,[1] Masashi Narazaki,[1] Hideki Tsuboi,[3] Yukihiko Saeki,[3] Tetsuya Tomita,[1] Toshio Tanaka,[1] and Atsushi Kumanogoh[1]

***Objective.*** **Semaphorin 4D (Sema4D)/CD100 has pleiotropic roles in immune activation, angiogenesis, bone metabolism, and neural development. We undertook this study to investigate the role of Sema4D in rheumatoid arthritis (RA).**

***Methods.*** **Soluble Sema4D (sSema4D) levels in serum and synovial fluid were analyzed by enzyme-linked immunosorbent assay. Cell surface expression and transcripts of Sema4D were analyzed in peripheral blood cells from RA patients, and immunohistochemical staining of Sema4D was performed in RA synovium. Generation of sSema4D was evaluated in an ADAMTS-4–treated monocytic cell line (THP-1 cells). The efficacy of anti-Sema4D antibody was evaluated in mice with collagen-induced arthritis (CIA).**

***Results.*** **Levels of sSema4D were elevated in both serum and synovial fluid from RA patients, and disease activity markers were correlated with serum sSema4D levels. Sema4D-expressing cells also accumulated in RA synovium. Cell surface levels of Sema4D on CD3+ and CD14+ cells from RA patients were reduced, although levels of *Sema4D* transcripts were unchanged. In addition, ADAMTS-4 cleaved cell surface Sema4D to generate sSema4D in THP-1 cells. Soluble Sema4D induced tumor necrosis factor α (TNFα) and interleukin-6 (IL-6) production from CD14+ monocytes. IL-6 and TNFα induced ADAMTS-4 expression in synovial cells. Treatment with an anti-Sema4D antibody suppressed arthritis and reduced proinflammatory cytokine production in CIA.**

***Conclusion.*** **A positive feedback loop involving sSema4D/IL-6 and TNFα/ADAMTS-4 may contribute to the pathogenesis of RA. The inhibition of arthritis by anti-Sema4D antibody suggests that Sema4D represents a potential therapeutic target for RA.**

Rheumatoid arthritis (RA) is a common autoimmune disease that causes chronic inflammation of the synovium. RA synovitis evokes arthritis symptoms and leads to destruction of cartilage and bone in joints.

Supported by research grants and Center of Innovation program (COI-STREAM) grants from the Ministry of Education, Culture, Sports, Science, and Technology of Japan, a Grant-in-Aid for Scientific Research from the Japan Society for the Promotion of Science (JSPS KAKENHI grant 25460495 to Dr. Ogata), grants-in-aid from the Ministry of Health, Labor, and Welfare (to Dr. Kumanogoh), and a Core Research for Evolutionary Science and Technology (CREST) grant from the Japan Science and Technology Agency (to Dr. Kumanogoh).

[1]Yuji Yoshida, MD, Atsushi Ogata, MD, PhD, Sujin Kang, PhD, Kousuke Ebina, MD, PhD, Satoshi Nojima, MD, PhD, Tetsuya Kimura, MD, Daisuke Ito, MD, Keiko Morimoto, MD, Masayuki Nishide, MD, Takashi Hosokawa, MD, Toru Hirano, MD, PhD, Yoshihito Shima, MD, PhD, Masashi Narazaki, MD, PhD, Tetsuya Tomita, MD, PhD, Toshio Tanaka, MD, PhD, Atsushi Kumanogoh, MD, PhD: Osaka University Graduate School of Medicine, Osaka, Japan; [2]Kenrin Shi, MD, PhD: Osaka University Graduate School of Medicine and Osaka University Hospital, Osaka, Japan; [3]Hideki Tsuboi, MD, PhD, Yukihiko Saeki, MD, PhD: National Hospital Organization Osaka Minami Medical Center, Osaka, Japan.

Address correspondence to Atsushi Ogata, MD, PhD, Department of Respiratory Medicine, Allergy, and Rheumatic Diseases, Osaka University Graduate School of Medicine, 2-2 Yamada-Oka, Suita, Osaka 565-0871, Japan. E-mail: ogata@imed3.med.osaka-u.ac.jp.

Submitted for publication September 22, 2014; accepted in revised form February 19, 2015.

Recent advances in understanding the pathogenesis of RA have revealed that complex interplay between genetic and environmental factors evoke autoimmunity, accompanied by the production of critical autoantigens such as citrullinated proteins (1,2). Once RA has developed, autoimmunity is sustained and leads to persistent synovitis, which in turn causes destruction of bone and cartilage (3,4). The mechanisms of sustained synovitis remain unclear. Recently, proinflammatory cytokines such as tumor necrosis factor $\alpha$ (TNF$\alpha$) and interleukin-6 (IL-6) were shown to have key roles in RA. Biologic disease-modifying antirheumatic drugs (DMARDs), which can block these cytokines, constitute the current standard of care (5,6). However, a substantial proportion of RA patients still do not achieve drug-free remission of their disease with biologic DMARDs. In order for RA patients to achieve true remission of their disease, it will be necessary to identify another key molecular player that contributes to autoimmunity, immune activation, and bone destruction in RA.

Semaphorins were originally identified as neural guidance factors (7). The semaphorin family consists of more than 20 proteins, categorized into 8 subclasses based on their structural features (8). Recent research on semaphorins demonstrated that these proteins have pleiotropic roles, including regulation of immune responses (9,10), angiogenesis (11,12), tumor metastasis (13,14), and bone metabolism (15–17). Semaphorins involved in various aspects of immune responses are referred to as "immune semaphorins" (18). Previous studies have shown that immune semaphorins have important roles in immunologic disorders, including multiple sclerosis (MS), airway hypersensitivity, granulomatosis with polyangiitis (Wegener's) (GPA), and RA (9,10). For instance, the level of soluble semaphorin 4A (sSema4A) is elevated in the serum of MS patients, in which Th17 cell populations are also increased (19). Recently, a *SEMA6A* variant was identified as a significant contributor to the risk of GPA (20). In addition, serum levels of Sema3A and Sema5A have been suggested to be relevant to RA (21–23). However, the pathologic significance of semaphorins in autoimmunity remains unclear.

Sema4D/CD100 was the first semaphorin shown to have a role in the immune system (24–26), and it was originally identified as a T cell activation marker (24). Indeed, Sema4D is abundantly expressed on the surface of T cells (24); however, it is also expressed in a broad range of hematopoietic cells. Although Sema4D is a membrane-bound protein, it also exists as a functional soluble form (sSema4D) following proteolytic cleavage upon cellular activation (27,28). Sema4D binds several receptors, plexin B1/B2, CD72, and plexin C1, which mediate the effects of Sema4D on neural cells, immune cells, endothelial cells, and epithelial cells (25,29). Several studies have demonstrated that Sema4D has crucial roles in the immune system. For example, Sema4D promotes activation of B cells and antibody production by B cells (30), Sema4D expressed on dendritic cells (DCs) is involved in antigen-specific T cell priming (31), Sema4D induces cytokine production by monocytes (32), and Sema4D mediates retrograde signals in mediating restoration of epithelium integrity (29).

Several studies have shown that Sema4D is relevant to the pathogenesis of autoimmunity. For instance, Sema4D-deficient mice are resistant to the development of experimental autoimmune encephalomyelitis (33), a murine model of MS. Sema4D is expressed on tumor-associated macrophages, and Sema4D produced by tumor-associated macrophages is involved in tumor angiogenesis and vessel maturation (34). Notably, Sema4D derived from osteoclasts suppresses bone formation by osteoblasts, and blocking of Sema4D results in increased bone mass (15). Immune abnormality, angiogenesis, and bone destruction all have critical roles in the progression of RA (35,36), suggesting that Sema4D might exacerbate RA. However, the involvement of Sema4D in the pathogenesis of RA has not yet been determined.

In this study, we found that sSema4D levels were elevated in serum and synovial fluid from RA patients. The increased levels of sSema4D were produced by an inflammation-related proteolytic mechanism, and the resultant sSema4D in turn induced inflammation, suggesting the existence of an inflammatory activation loop in RA synovium. Inhibition of Sema4D ameliorated the symptoms of collagen-induced arthritis (CIA). These results suggest that Sema4D represents a potential target for treatment of RA.

## SUBJECTS AND METHODS

**Subjects.** Blood samples were obtained from 101 patients with RA, 34 with systemic lupus erythematosus (SLE), 10 with ankylosing spondylitis (AS), and 10 with osteoarthritis (OA) at Osaka University Hospital and National Hospital Organization Osaka Minami Medical Center. Patients with RA were diagnosed according to the 1987 revised criteria of the American College of Rheumatology (37). Blood samples were also obtained from healthy individuals recruited from university staff, hospital staff, and the student population. Seven RA and 10 OA synovial tissue samples were obtained from patients undergoing synovectomy or knee replacement, and RA and OA synovial fluid samples were obtained from patients undergoing knee arthrocentesis. All samples were obtained after informed consent was provided by the subjects in accordance with the Declaration of Helsinki and with approval from the local ethics committees of Osaka University Hospital and National Hospital Organization Osaka Minami Medical Center.

This study was registered in the University Hospital Medical Information Network Clinical Trials Registry (UMIN000013076).

**Enzyme-linked immunosorbent assays (ELISAs).** Soluble Sema4D levels in serum and synovial fluid samples and cell culture supernatants were measured using an ELISA kit (MyBioSource). Serum and synovial fluid samples were stored at −20°C prior to ELISAs. The lower detection limit of sSema4D was 125 pg/ml. Levels of ADAMTS-4 in serum and synovial fluid samples were also determined using an ELISA kit (MyBioSource). The concentrations of human TNFα and IL-6 in culture supernatants were determined using DuoSet ELISA kits for each cytokine (R&D Systems).

**Histology.** Immunohistochemical staining was performed on 7 RA and 10 OA synovial tissue samples. Briefly, sections were deparaffinized and subjected to antigen retrieval by autoclaving in 10 m*M* citrate buffer (pH 6.0) for 15 minutes at 125°C, after which endogenous peroxidase activity was blocked with Dako REAL peroxidase blocking solution. Sections were allowed to react overnight with mouse anti-Sema4D polyclonal antibody (1:100; BD Biosciences), mouse anti-CD3 monoclonal antibody (1:100; Dako), Ready-to-Use mouse anti-CD20 monoclonal antibody (1:1; Dako), and Ready-to-Use mouse negative control Ig cocktail (1:1; Dako) or rabbit anti-CD31 polyclonal antibody (1:50; Abcam). Slides were then incubated with a peroxidase-labeled polymer conjugated to secondary anti-rabbit antibodies using EnVisionTM1/HRP (Dako) and then developed with 3,3′-diaminobenzidine as the chromogen.

Histologic analyses were performed on joints from mice with CIA. Hindlimb specimens from mice were fixed in 4% paraformaldehyde (Wako Pure Chemical) and decalcified. Hematoxylin and eosin and Safranin O staining were used to assess synovitis.

**Cell preparations.** Human peripheral blood mononuclear cells (PBMCs) were separated by density-gradient centrifugation using Ficoll-Paque Plus (GE Healthcare Bio-Sciences). CD14+ monocytes were collected using CD14 MicroBeads (Miltenyi Biotec), yielding >90% CD14+ cells.

**Flow cytometry.** PBMCs were prepared in heparinized tubes by Ficoll-Paque density-gradient centrifugation and then analyzed on a FACSCanto (BD Biosciences) using FlowJo software (Tree Star). To prevent nonspecific binding, cells ($2 \times 10^5$) were incubated with human AB serum (Lonza) for 45 minutes at 4°C and then labeled with antibodies against indicated cell surface antigens. The following antibodies were used: fluorescein isothiocyanate–conjugated anti-human Sema4D (A8; BioLegend), phycoerythrin (PE)–conjugated anti-human CD3 (HIT3a; BioLegend), PE-conjugated anti-human CD14 (M5E2; BioLegend), and PE-conjugated anti-human CD19 (HIB19; Tonbo Biosciences).

**Quantitative reverse transcription–polymerase chain reaction (qRT-PCR).** CD3+, CD19+, or CD14+ cells ($1 \times 10^4$) were sorted using a FACSAria (BD Biosciences). Total RNA was extracted using an RNeasy Mini kit (Qiagen), and complementary DNA (cDNA) was synthesized using a SuperScript II cDNA synthesis kit (Invitrogen). Quantitative RT-PCR analysis was performed on a 7900HT Fast Real-Time PCR system (Applied Biosystems) using a TaqMan PCR protocol. Assay ID numbers for TaqMan primer sets (Applied Biosystems) were Hs00174819_m1 for human *SEMA45* and HS00192708_m1 for human *ADAMTS4*. Expression levels of tested genes were normalized to that of the housekeeping gene *ACTB* (Hs01060665_g1) and calculated using the $\Delta C_t$ method.

**Shedding of sSema4D.** The monocytic cell line THP-1 and PBMCs from RA patients were cultured at 37°C for 12 hours in 96-well plates at a density of $5 \times 10^6$ cells/ml in RPMI 1640 medium containing 10 μg/ml of matrix metalloproteinase 3 (MMP-3; Sigma-Aldrich), MMP-9 (R&D Systems), ADAM-17 (R&D Systems), and ADAMTS-4 (R&D Systems). Soluble Sema4D concentrations were measured using an ELISA kit (MyBioSource).

**Isolation of synovial cells and stimulation by IL-6 and TNFα.** Samples of knee articular synovium were obtained from RA patients. Synovial tissues were chopped finely and then digested for 45 minutes with continuous stirring at 37°C with collagenase D (800 Mandl units/ml; Roche) and dispase I (10 mg/ml; Invitrogen) in RPMI 1640 medium containing 5% fetal calf serum (FCS). After digestion, the samples were filtered through a cell strainer (BD Biosciences). Adherent synovial cells were harvested and passaged into another dish. For experiments, synovial cells at passages 2–3 were seeded in 96-well plates at $1 \times 10^5$ cells per well and then stimulated for 2 days with 1 μg/ml of IL-6 and 0.1 μg/ml of TNFα (PeproTech) in Dulbecco's modified Eagle's medium containing 10% FCS. At the end of the stimulation period, cells were collected, and messenger RNA (mRNA) was extracted. Quantitative RT-PCR analysis of ADAMTS-4 was performed as described above. Concentrations of ADAMTS-4 in culture supernatants were also measured by ELISA.

**Monocyte culture and cytokine assays.** CD14+ monocytes from RA patients ($1 \times 10^5$) were stimulated with or without various concentrations of soluble human Sema4D-Fc fusion protein, naturally cleaved sSema4D, or CD72 ligation antibody (BU40; Santa Cruz Biotechnology). For blocking experiments, cells were cocultured with 1 μg/ml of naturally cleaved Sema4D and 10 μg/ml of anti-Sema4D/CD100 antibody (3E9) (33) or isotype-matched control IgG for 48 hours. Concentrations of human TNFα and IL-6 in culture supernatants were determined by ELISA.

Human Sema4D-Fc fusion protein and sSema4D were produced and purified as previously described (28,32), and Recombinant Human IgG1 Fc (R&D Systems) was used as a control. Naturally cleaved sSema4D was affinity-purified using a column containing CNBr-activated Sepharose 4 Fast Flow resin (Amersham Pharmacia Biotech) conjugated to anti-Sema4D monoclonal antibody (A8) as described previously (28).

**Induction and assessment of CIA.** Eight-week-old male DBA/1J mice were purchased from Oriental Yeast Company. Bovine type II collagen (2 mg/ml; Chondrex) was dissolved in 0.05*M* acetic acid and emulsified with an equal volume of Freund's complete adjuvant (Sigma-Aldrich). Mice were immunized by intradermal injection at the base of the tail with 100 μl (2 mg/ml) of the emulsion (day 0). Booster injections of 100 μl of emulsion consisting of equal parts of Freund's incomplete adjuvant (Sigma-Aldrich) and 2 mg/ml type II collagen in 0.05*M* acetic acid were administered at another site at the base of the tail on day 21. Mice with CIA received intraperitoneal injections of 50 mg/kg anti-Sema4D antibody (BMA-12) (30) (n = 6), 25 mg/kg anti-Sema4D antibody (n = 8), or isotype control antibodies (Chugai Pharmaceutical) on day 28 and day 35. Serum was collected on day 42. Serum levels of IL-6, TNFα, and IL-1β were determined using a Bio-Plex Pro Mouse Cytokine Assay (Bio-Rad).

Serum titers of anti–type II collagen antibodies were detected by ELISA (Chondrex). Arthritis clinical scores were determined on a scale of 0–4 for each paw (0 = normal;

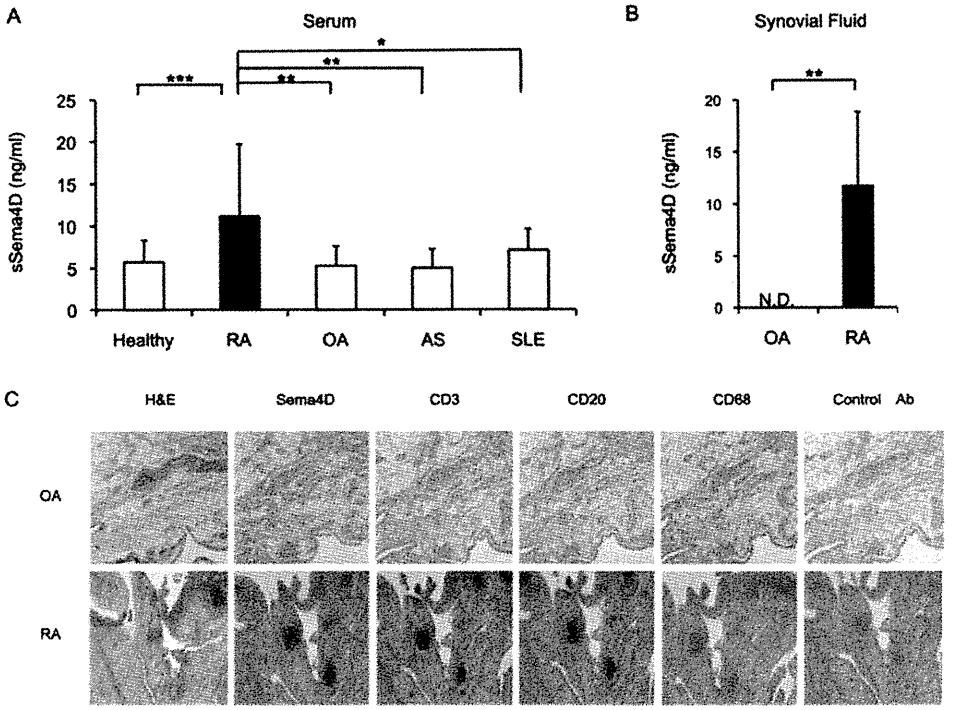


**Figure 1.** Levels of soluble semaphorin 4D (sSema4D) in serum and synovial fluid samples from patients with rheumatoid arthritis (RA), and Sema4D protein expression in RA synovium. **A,** Soluble Sema4D levels in serum samples from healthy individuals and from 101 patients with RA, 10 patients with osteoarthritis (OA), 10 patients with ankylosing spondylitis (AS), and 34 patients with systemic lupus erythematosus (SLE). **B,** Levels of sSema4D in synovial fluid samples from 7 RA patients and 10 OA patients. Values in **A** and **B** are the mean ± SD. ND = not detectable. * = $P < 0.05$; ** = $P < 0.01$; *** = $P < 0.001$. **C,** Hematoxylin and eosin (H&E) staining and immunohistochemical staining for Sema4D, CD3, CD20, and CD68 in synovial tissue samples from patients with OA or RA. Images shown are representative of samples from 7 RA patients and 10 OA patients. Original magnification × 40. Ab = antibody.

1 = erythema and swelling of 1 digit; 2 = erythema and swelling of 2 digits or erythema and swelling of the ankle joint; 3 = erythema and swelling of 3 digits or swelling of 2 digits and the ankle joint; and 4 = erythema and severe swelling of the ankle, foot, and digits with deformity). Two paws of each mouse were evaluated histologically. Joint pathology was assessed and quantitated as described previously (38). The paws of mice treated with anti-Sema4D antibody (n = 12), control antibody (n = 12), or no antibody (n = 12) were stained with anti-CD31 antibodies. Vessels were counted manually in 5 fields (40×) per paw and averaged. The experimental protocol was approved by the Institutional Animal Care and Use Committee of Osaka University.

**Statistical analysis.** Data are expressed as the mean ± SD or mean ± SEM. Nonparametric Mann-Whitney U tests were used to compare 2 groups, and comparisons between 3 groups were performed using the Kruskal-Wallis test followed by the Mann-Whitney U test. $P$ values less than or equal to 0.05 were considered significant. Correlations between clinical parameters and serum sSema4D levels were determined using Pearson's correlation coefficient (r).

## RESULTS

**Elevation of sSema4D levels in RA, and accumulation of Sema4D-expressing cells in RA synovium.** To investigate the pathologic implications of Sema4D in RA, we first measured the serum concentrations of Sema4D in patients with several autoimmune and joint-destructive diseases. As shown in Figure 1A, serum sSema4D levels were significantly higher in RA patients than in healthy individuals (mean ± SD 11.2 ± 8.4 ng/ml versus 5.6 ± 2.7 ng/ml; $P < 0.001$) (demographics and characteristics of RA patients are shown in Supplementary Table 1, available on the *Arthritis & Rheumatology* web site at http://onlinelibrary.wiley.com/doi/10.1002/art.39086/abstract). In contrast, serum sSema4D levels were not elevated in patients with OA, AS, or SLE (mean ± SD 5.2 ± 2.4 ng/ml, 4.9 ± 2.3 ng/ml, and 7.0 ± 2.6 ng/ml, respectively). Notably, Sema4D levels were also

elevated in the synovial fluid of RA patients (mean ± SD 11.8 ± 7.0 ng/ml), but Sema4D was undetectable in the synovial fluid of OA patients ($P < 0.01$) (Figure 1B).

Immunohistochemical staining revealed accumulation of Sema4D-positive cells in RA synovium, clustered mainly in follicle-like germinal centers. However, such accumulation and clustering of Sema4D-expressing cells were not observed in OA synovium (Figure 1C). CD3 and CD20 were colocalized in Sema4D-stained follicle-like germinal centers, indicating that the Sema4D-expressing cells were synovial infiltrating lymphocytes (see Supplementary Figure 1, available on the *Arthritis & Rheumatology* web site at http://onlinelibrary.wiley.com/doi/10.1002/art.39086/abstract). In contrast, CD68+ macrophages faintly expressed Sema4D. Additionally, the distribution of CD68+ cells was patchy, and their localization patterns were different from those of T and B cells.

**Correlation of serum sSema4D levels with RA disease activity and biomarkers.** To determine the clinical implications of sSema4D, we examined the correlations between serum sSema4D levels and clinical features. Table 1 summarizes the correlations between patients' clinical features and serum sSema4D levels. There were no apparent correlations between sSema4D levels and age, sex, disease duration, or medications (data not shown). In contrast, serum sSema4D levels were positively correlated with disease activity markers such as the Disease Activity Score in 28 joints (DAS28) (39) ($r = 0.383$, $P < 0.01$), the C-reactive protein (CRP) level ($r = 0.346$, $P < 0.01$), and the rheumatoid factor (RF) titer ($r = 0.328$, $P < 0.01$). In addition, levels of bone metabolic markers such as bone alkaline phosphatase (BAP) ($r = 0.255$, $P < 0.05$) and urinary deoxypyridinoline ($r = 0.318$, $P < 0.05$) correlated with serum sSema4D levels.

**Table 1.** Correlations between levels of soluble semaphorin 4D and clinical features in the 101 patients with rheumatoid arthritis*

| Category, feature | r | *P* |
|---|---|---|
| Clinical disease activity (DAS28) | 0.383 | <0.01 |
| Autoantibodies | | |
| RF | 0.328 | <0.01 |
| ACPA | −0.041 | NS |
| Biomarkers | | |
| CRP | 0.346 | <0.01 |
| MMP-3 | 0.055 | NS |
| Bone turnover markers | | |
| BAP | 0.255 | <0.05 |
| Osteocalcin | 0.092 | NS |
| Urinary deoxypyridinoline | 0.318 | <0.05 |
| ICTP | 0.091 | NS |
| Serum NTX | 0.026 | NS |
| Spine DXA | −0.145 | NS |

* DAS28 = Disease Activity Score in 28 joints; RF = rheumatoid factor; ACPA = anti–citrullinated protein antibody; NS = not significant; CRP = C-reactive protein; MMP-3 = matrix metalloproteinase 3; BAP = bone alkaline phosphatase; ICTP = C-terminal crosslinking telopeptide of type I collagen; NTX = N-telopeptide of type I collagen; DXA = dual x-ray absorptiometry.

Scatterplots confirmed the relationships between serum levels of sSema4D and these disease activity markers (Figure 2A). Sequential analysis of serum sSema4D levels was performed in RA patients treated with biologic DMARDs (n = 17); specifically, serum levels of sSema4D were evaluated before and 6 months after initiation of biologic DMARD therapy (14 patients were treated with TNF inhibitors, and 3 patients were treated with tocilizumab). A significant decrease in serum sSema4D levels after biologic DMARD treatment was observed in patients who were good responders according to the European League Against Rheumatism response criteria (40) (Figure 2B). In contrast, sSema4D levels were not changed in patients with a moderate response or no response (Figure 2B). The posttreatment change ratio of Sema4D after biologic DMARD treatment was significantly correlated with the change ratio of the DAS28 ($r = 0.799$, $P < 0.001$) (Figure 2C), suggesting the involvement of Sema4D in determining the clinical status of RA. The reductions in serum sSema4D levels did not differ significantly between patients treated with TNF inhibitors and those treated with an IL-6 inhibitor. Thus, the reduction in serum sSema4D levels simply correlated with reduction in disease activity.

**Shedding of Sema4D in RA patients.** Sema4D is abundantly expressed in T cells but weakly expressed in other cell types such as B cells (24). Sema4D is also expressed on antigen-presenting cells, including macrophages and DCs (32). As shown in Figure 1C, we observed Sema4D-expressing cells in the synovium. Next, we examined Sema4D expression in PBMCs from RA patients and healthy individuals. In healthy individuals, cell surface Sema4D was expressed abundantly on CD3+ and CD14+ cells and at lower levels on CD19+ cells (Figure 3A). Furthermore, the cell surface expression of Sema4D was down-regulated on all cells from RA patients, especially on cells positive for CD3 or CD14. In contrast, qRT-PCR revealed that the expression of mRNA for Sema4D was not reduced in RA patients (Figure 3B), suggesting that the reduction in cell surface Sema4D was due to shedding of Sema4D from the cell surface.

Previous studies showed that although Sema4D is a membrane-bound protein, it can be cleaved from the cell surface by metalloproteinases to yield a soluble form (27). Therefore, we examined the proteolytic cleavage of Sema4D. ADAMs, ADAMTS, and MMPs are proteolytic enzymes that digest extracellular matrix proteins such as collagen, and they process bioactive substances that have a physiologic role in RA (41). We incubated

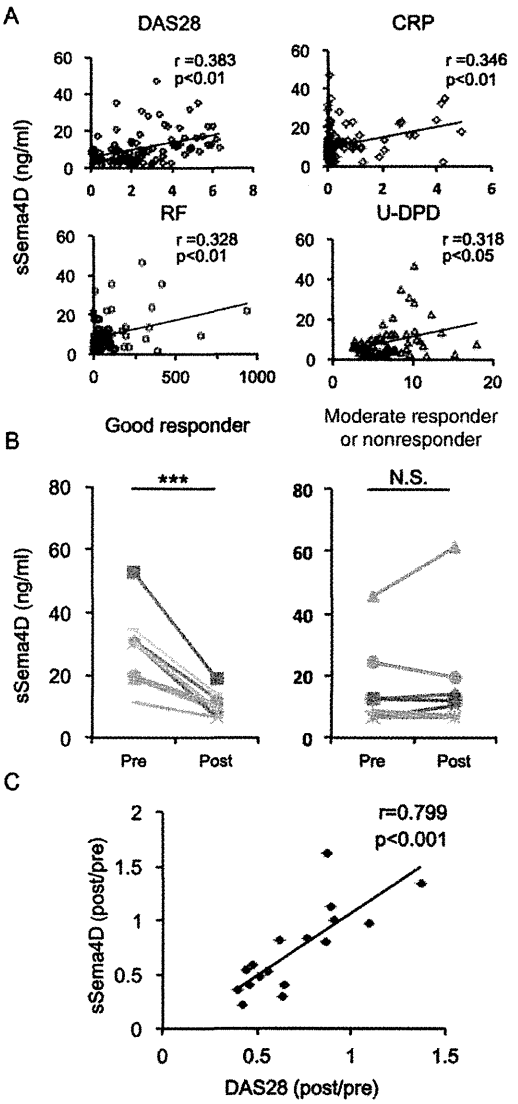


**Figure 2.** Correlations of serum levels of soluble semaphorin 4D (sSema4D) with markers of rheumatoid arthritis disease activity. **A,** Positive correlation of serum sSema4D levels with the Disease Activity Score in 28 joints (DAS28), the C-reactive protein (CRP) level, the rheumatoid factor (RF) titer, and the level of urinary deoxypyridinoline (u-DPD). **B,** Serum sSema4D levels before and after biologic disease-modifying antirheumatic drug (DMARD) treatment in 9 good responders and 8 moderate responders or nonresponders according to the European League Against Rheumatism response criteria. *** = $P < 0.001$. NS = not significant. **C,** Correlation of change ratio in serum sSema4D levels with change ratio of DAS28 after treatment with biologic DMARDs (n = 17 samples).

Sema4D-expressing cells (THP-1 cells) with recombinant metalloproteinases including MMP-3, MMP-9, ADAM-17, and ADAMTS-4, and then we measured

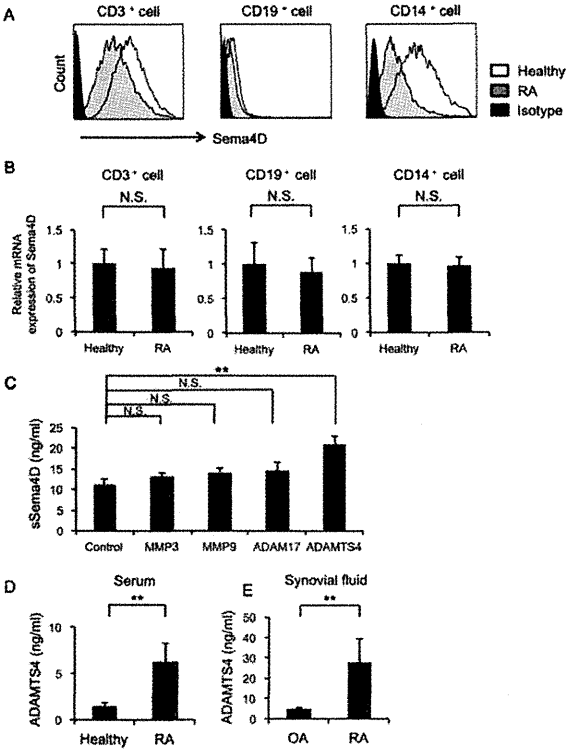


**Figure 3.** Semaphorin 4D (Sema4D) expression, and soluble Sema4D (sSema4D) production with ADAMTS-4 as the sheddase. **A,** Histograms of cell surface expression of Sema4D in peripheral blood CD3+, CD19+, and CD14+ cells. Results shown are representative of findings from 5 rheumatoid arthritis (RA) patients and 5 healthy individuals. **B,** Expression of mRNA for Sema4D in peripheral blood CD3+, CD19+, and CD14+ cells. Results shown are from 5 RA patients and 5 healthy individuals. **C,** Levels of sSema4D in culture supernatant of THP-1 cells cultured with recombinant matrix metalloproteinase 3 (MMP-3), MMP-9, ADAM-17, and ADAMTS-4 (n = 5 samples per group). Results are representative of 3 independent experiments. **D,** Serum levels of ADAMTS-4 in 20 RA patients and 16 healthy individuals. **E,** Synovial fluid levels of ADAMTS-4 in 7 RA patients and 10 osteoarthritis (OA) patients. Values in **B–E** are the mean ± SEM. ** = $P < 0.01$. NS = not significant.

sSema4D levels in the culture supernatants. ADAMTS-4 significantly induced the release of sSema4D into the culture supernatant (Figure 3C) (see Supplementary Figure 2, available on the *Arthritis & Rheumatology* web site at http://onlinelibrary.wiley.com/doi/10.1002/art.39086/abstract). Consistent with this, we detected elevated levels of ADAMTS-4 in serum and synovial fluid in the RA patients examined in this study (Figures 3D and E).

**Proinflammatory cytokine production by sSema4D.** To determine the pathogenic role of elevated sSema4D levels in RA, we investigated the effect

of sSema4D on TNFα and IL-6 production. Treatment with naturally cleaved sSema4D increased production of TNFα and IL-6 by CD14+ monocytes in a dose-dependent manner (Figure 4A). In addition, recombinant sSema4D-Fc fusion protein also induced TNFα and IL-6 production by PBMCs in a dose-dependent manner (see Supplementary Figure 3, available on the *Arthritis & Rheumatology* web site at http://onlinelibrary.wiley.com/doi/10.1002/art.39086/abstract). Moreover, anti-Sema4D antibody suppressed TNFα and IL-6 production induced by sSema4D (Figure 4B). CD72 is a receptor for Sema4D, and a CD72 ligation antibody also induced TNFα and IL-6 production in CD14+ monocytes, in which Sema4D induced dephosphorylation of CD72 (see Supplementary Figures 4 and 5, available on the *Arthritis & Rheumatology* web site at http://onlinelibrary.wiley.com/doi/10.1002/art.39086/abstract).

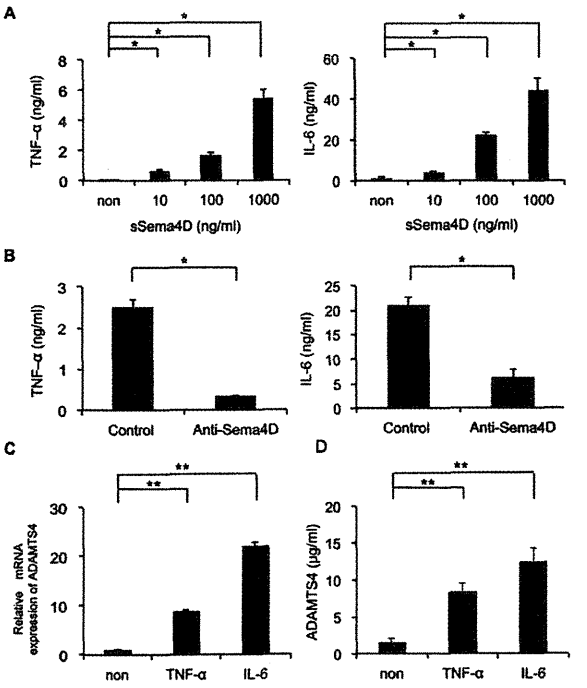


**Figure 4.** Inflammatory cytokine production induced by semaphorin 4D (Sema4D), and elevated ADAMTS-4 expression by inflammatory cytokines. **A,** Tumor necrosis factor α (TNFα) and interleukin-6 (IL-6) levels in culture supernatant of CD14+ monocytes from rheumatoid arthritis (RA) patients after stimulation with naturally cleaved soluble Sema4D (sSema4D) for 72 hours. Results shown are representative of 3 independent experiments. **B,** TNFα and IL-6 levels in culture supernatant of CD14+ monocytes from RA patients after stimulation with naturally cleaved sSema4D for 48 hours with or without anti-Sema4D antibody. Results shown are representative of 3 independent experiments. **C** and **D,** Elevated expression of ADAMTS-4 mRNA (**C**) and elevated ADAMTS-4 protein levels (**D**) in primary cultures of TNFα- and IL-6–stimulated synovial cells from RA patients. Data were compiled from 5 independent experiments. Values are the mean ± SEM. * = $P < 0.05$; ** = $P < 0.01$. non = not stimulated.

Because previous studies showed that inflammatory cytokines induce ADAMTS-4 in synovial cells (42), we examined ADAMTS-4 production in TNFα- and IL-6–stimulated synovial cells. TNFα and IL-6 treatment increased mRNA and protein levels of ADAMTS-4 (Figures 4C and D). These results not only indicated that sSema4D can induce the production of proinflammatory cytokines but also implied that such cytokines in turn upregulate the cleavage of Sema4D by ADAMTS-4.

**Amelioration of CIA severity by blocking of Sema4D.** To determine the pathologic roles of Sema4D in arthritis, we examined the effect of anti-Sema4D antibody treatment on CIA. Arthritis scores in anti-Sema4D antibody–treated mice were significantly lower than those in control mice (Figure 5A), and the decrease in arthritis scores was attenuated in mice treated with half a dose of antibody (see Supplementary Figure 6, available on the *Arthritis & Rheumatology* web site at http://onlinelibrary.wiley.com/doi/10.1002/art.39086/abstract). Histologic analysis revealed that blocking Sema4D in mice with CIA also reduced inflammatory infiltration into the synovium, decreased pannus formation, and ameliorated erosion of adjacent cartilage and bone (Figure 5B). Histologic scores in the joints of anti-Sema4D antibody–treated mice were significantly reduced (Figure 5C). Furthermore, serum TNFα and IL-6 levels on day 42 were significantly reduced in anti-Sema4D antibody–treated mice (Figure 5D). We evaluated angiogenesis by antibody staining for CD31, a marker of blood vessel endothelium. Mice treated with anti-Sema4D antibody exhibited poor induction of angiogenesis at sites of inflammation (see Supplementary Figures 7A and B, available on the *Arthritis & Rheumatology* web site at http://onlinelibrary.wiley.com/doi/10.1002/art.39086/abstract). Additionally, the serum level of anticollagen antibody was reduced in these animals (see Supplementary Figure 8, available on the *Arthritis & Rheumatology* web site at http://onlinelibrary.wiley.com/doi/10.1002/art.39086/abstract).

## DISCUSSION

In this study, we investigated the clinical implications of sSema4D in RA. Levels of sSema4D were elevated in RA serum and synovial fluid. However, sSema4D levels were not elevated in OA and SLE, suggesting that

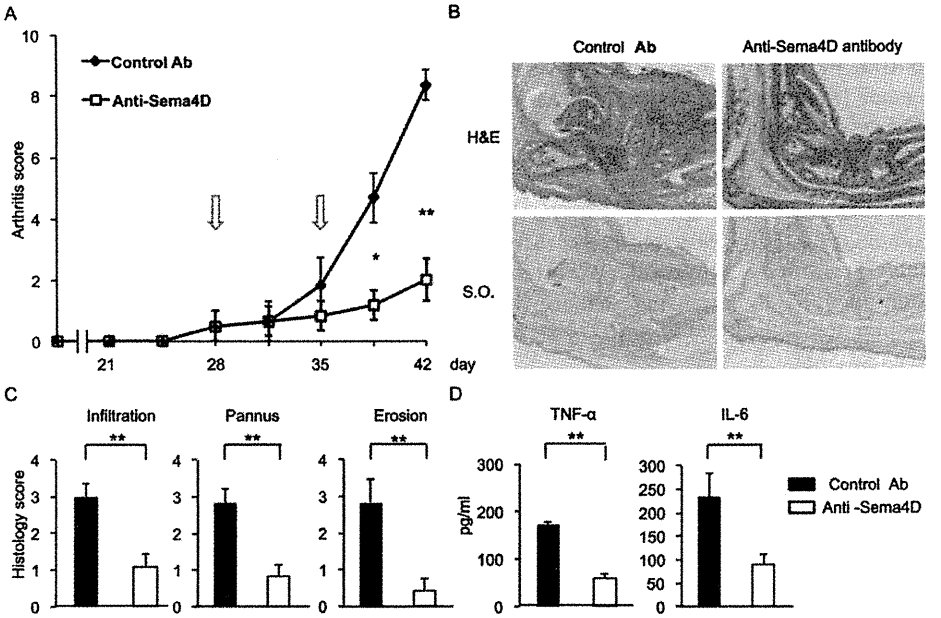


**Figure 5.** Blocking of semaphorin 4D (Sema4D) ameliorates severity of collagen-induced arthritis (CIA) in mice. **A,** Average arthritis scores of mice with CIA. Anti-Sema4D or control antibody (Ab) (50 mg/kg) was administered intraperitoneally on days 28 and 35 (**arrows**) (n = 6 mice per group). Data are representative of 3 independent experiments. **B,** Sections of a mouse ankle joint on day 42 after first immunization. Sections were stained with hematoxylin and eosin (H&E) or Safranin O (SO). Original magnification × 100. **C,** Average pathologic scores of paw sections on day 42 (n = 6 mice per group). **D,** Serum levels of tumor necrosis factor α (TNFα) and interleukin-6 (IL-6) on day 42 (n = 6 mice per group). Values are the mean ± SEM and are representative of 3 independent experiments. * = $P < 0.05$; ** = $P < 0.01$.

high sSema4D levels are specifically associated with RA. Serum sSema4D levels correlated with known clinical and biologic markers of RA (Table 1). In particular, serum sSema4D levels correlated with the DAS28, the CRP level, the RF titer, and the urinary deoxypyridinoline level in RA patients. Successful treatment of RA reduced serum sSema4D levels, and reductions in the sSema4D level were significantly correlated with reductions in clinical disease activity as measured by the DAS28. Collectively, these results suggest that sSema4D is a potentially useful biomarker for RA disease activity. In addition, serum sSema4D levels were correlated with levels of CRP, a well-known acute-phase protein induced by proinflammatory cytokines such as IL-1β, IL-6, and TNFα (43). Because sSema4D induced IL-6 and TNFα production from CD14+ monocytes, it is possible that sSema4D affects CRP production via induction of IL-6 and TNFα in RA patients. The RF titer was also correlated with serum sSema4D levels. Given that Sema4D has been implicated in activation of B cells and antibody production (28,31), sSema4D may be directly relevant to RF production.

Recent work showed that Sema4D expressed in osteoclasts inhibits bone regeneration by inhibiting osteoblasts (15). Consistent with this, we found that some bone metabolic markers were correlated with serum sSema4D levels in RA (Table 1). The bone formation marker BAP and the bone resorption marker urinary deoxypyridinoline were correlated with serum sSema4D levels. However, other bone formation markers (such as osteocalcin) and bone resorption markers (such as C-terminal crosslinking telopeptide of type I collagen and serum N-telopeptide of type I collagen) were not correlated with serum sSema4D levels. The relationship between serum sSema4D levels and bone metabolic markers in RA patients is a subject of controversy, although the local concentration of Sema4D may be relevant to joint destruction in RA. Further studies will be needed to determine the importance of Sema4D in bone destruction in RA.

Because Sema4D is strongly expressed in immune cells (24), we initially assumed that elevated expression of *SEMA4D* explained the increase in sSema4D in RA serum and synovial fluid. Contrary to our expectation, however, fluorescence-activated cell sorting analysis revealed that levels of Sema4D were actually reduced in lymphocytes and monocytes from the peripheral blood of RA patients. Because expression of Sema4D mRNA was stable in all cells, it is likely that

the relative reduction in cellular levels of Sema4D was due to cleavage and shedding of Sema4D from the cell surface. In support of this notion, a previous study showed that EDTA, an inhibitor of metalloproteinases, inhibits sSema4D secretion, suggesting that sSema4D is produced via a shedding mechanism (27). Other studies showed that ADAM-17 regulates Sema4D exodomain cleavage on activated platelets (44,45). Taken together, the results of these studies prompted us to investigate the generation and function of Sema4D.

We examined several proteolytic enzymes as candidate sheddases for sSema4D. Proteolytic enzymes such as ADAMTS, ADAMs, and MMPs influence inflammation and progression of arthritis (46–48). Herein we showed that induction of sSema4D is dependent on ADAMTS-4. Originally, ADAMTS-4 was considered to have a key role in the degradation of cartilage proteoglycan (aggrecan) in OA and RA. Consistent with this, levels of ADAMTS-4 were elevated in RA serum, and TNFα and IL-6 induced the production of ADAMTS-4.

In this study, we demonstrated that production of inflammatory cytokines such as TNFα and IL-6 increased upon stimulation with sSema4D. We also showed that sSema4D induced dephosphorylation of CD72 (see Supplementary Figure 5, available on the *Arthritis & Rheumatology* web site at http://onlinelibrary.wiley.com/doi/10.1002/art.39086/abstract). CD72 contains an immunoreceptor tyrosine–based inhibition motif in its cytoplasmic region (49). Investigators in our group have previously reported that Sema4D induces dephosphorylation of CD72, turning off its negative signal in B cells (32). It thus appears that Sema4D is involved in cytokine production in monocytes as well.

Our results indicated that sSema4D induces TNFα and IL-6 production and that both TNFα and IL-6 can induce ADAMTS-4, which is involved in generation of sSema4D. Therefore, we hypothesized that the vicious circle of sSema4D/TNFα/IL-6/ADAMTS-4 functions as an autocrine accelerator of the IL-6/TNFα inflammatory axis in RA. It is well known that TNFα and IL-6 induce osteoclastogenesis through RANKL production, and ADAMTS-4 induces cartilage degradation in RA (48). In addition, Sema4D inhibits bone formation (15). Therefore, the autocrine loop involving Sema4D induces cartilage destruction, inhibits bone regeneration, and evokes continuous inflammatory symptoms. This Sema4D loop may have a central role in RA inflammation and the associated joint destruction (see Supplementary Figure 9, available on the *Arthritis & Rheumatology* web site at http://onlinelibrary.wiley.com/doi/10.1002/art.39086/abstract).

We analyzed the effect of anti-Sema4D antibody treatment in a mouse model of inflammatory arthritis. Blocking Sema4D in CIA exerted favorable therapeutic effects, decreasing destruction of cartilage and bone, cell infiltration into the synovium, and production of TNFα and IL-6 (Figure 5). To investigate the therapeutic effects of anti-Sema4D antibody on ongoing arthritis, we administered anti-Sema4D antibody after arthritis had already commenced. These observations suggest that Sema4D represents a possible therapeutic target for treatment of RA. Recently developed biologic DMARDs inhibit TNFα and IL-6 function; however, these therapies do not inhibit cytokine production directly. Therefore, RA flares are often observed after cessation of biologic DMARD therapy. Thus, it seems likely that direct inhibition of TNFα and IL-6 production by anti-Sema4D therapy would be useful for RA management. An anti-Sema4D antibody is currently undergoing a phase I clinical trial (NCT01313065) in cancer patients (50). However, the long-term feasibility of anti-Sema4D antibody is still unknown. Careful and well-designed clinical applications will be needed.

In summary, we demonstrated that serum sSema4D levels are well correlated with known markers of clinical features and laboratory findings. The critical roles of Sema4D in RA pathogenesis suggest that Sema4D is a potential novel target for RA treatment.

## ACKNOWLEDGMENTS

We appreciate the patients and healthy volunteers who participated in this research.

## AUTHOR CONTRIBUTIONS

All authors were involved in drafting the article or revising it critically for important intellectual content, and all authors approved the final version to be published. Drs. Yoshida and Ogata had full access to all of the data in the study and take responsibility for the integrity of the data and the accuracy of the data analysis.

**Study conception and design.** Yoshida, Ogata, Kumanogoh.

**Acquisition of data.** Yoshida, Ogata, Ebina, Shi, Nojima, Kimura, Ito, Morimoto, Nishide, Hosokawa, Hirano, Shima, Narazaki, Tsuboi, Saeki, Tomita, Tanaka.

**Analysis and interpretation of data.** Yoshida, Ogata, Kang, Kumanogoh.

## REFERENCES

1. Kochi Y, Suzuki A, Yamamoto K. Genetic basis of rheumatoid arthritis: a current review. Biochem Biophys Res Commun 2014;452:254–62.
2. Holmdahl R, Malmstrom V, Burkhardt H. Autoimmune priming, tissue attack and chronic inflammation: the three stages of rheumatoid arthritis. Eur J Immunol 2014;44:1593–9.
3. Ogura H, Murakami M, Okuyama Y, Tsuruoka M, Kitabayashi C, Kanamoto M, et al. Interleukin-17 promotes autoimmunity by triggering a positive-feedback loop via interleukin-6 induction. Immunity 2008;29:628–36.
4. Zhao W, Zhang C, Shi M, Zhang J, Li M, Xue X, et al. The discoidin domain receptor 2/annexin A2/matrix metalloproteinase 13 loop promotes joint destruction in arthritis through promoting migration and invasion of fibroblast-like synoviocytes. Arthritis Rheumatol 2014;66:2355–67.
5. Cessak G, Kuzawinska O, Burda A, Lis K, Wojnar M, Mirowska-Guzel D, et al. TNF inhibitors: mechanisms of action, approved and off-label indications. Pharmacol Rep 2014;66:836–44.